

Review

Molecular Imaging of Bacterial Infections *in vivo*: The Discrimination between Infection and Inflammation

Heather Eggleston and Peter Panizzi *

Department of Drug Discovery and Development, Harrison School of Pharmacy, Auburn University, Auburn, AL 36849, USA; E-Mail: hce0001@auburn.edu (H.E.)

* Author to whom correspondence should be addressed; E-Mail: panizzi@auburn.edu;
Tel.: +1-334-844-7941; Fax: +1-334-844-8331.

Received: 18 March 2014; in revised form: 6 May 2014 / Accepted: 13 May 2014 /

Published: 30 May 2014

Abstract: Molecular imaging by definition is the visualization of molecular and cellular processes within a given system. The modalities and reagents described here represent a diverse array spanning both pre-clinical and clinical applications. Innovations in probe design and technologies would greatly benefit therapeutic outcomes by enhancing diagnostic accuracy and assessment of acute therapy. Opportunistic pathogens continue to pose a worldwide threat, despite advancements in treatment strategies, which highlights the continued need for improved diagnostics. In this review, we present a summary of the current clinical protocol for the imaging of a suspected infection, methods currently in development to optimize this imaging process, and finally, insight into endocarditis as a model of infectious disease in immediate need of improved diagnostic methods.

Keywords: molecular imaging; endocarditis; infection; inflammation; *Staphylococcus aureus*

1. Clinical Approach to Identification of Infection

Identification of generalized infection with imaging modalities relies upon monitoring morphological changes with radiographs, ultrasonography, computed tomography (CT), and magnetic resonance imaging (MRI). CT and MRI provide particularly useful data in detecting organ and musculoskeletal infections; however, the data collected from these imaging modalities is often only attainable in late stages of infection and is further complicated by morphological distortion induced by post-surgical changes, scarring, and presence of foreign materials [1]. Most imaging modalities are

further limited by their inability to distinguish (i) inflammation from infection; (ii) tumors from abscesses; and (iii) causative pathogens. There is a rich history of the use of radiolabeled markers (*i.e.*, proteins and cells) for imaging infectious processes by either single-photon emission computed tomography (SPECT) or positron emission tomography (PET) as a complement to these aforementioned techniques for morphological imaging. Examples of radiolabeling isotopes that are most common include ^{99m}Tc Technetium (^{99m}Tc), ^{111}In Indium (^{111}In), ^{68}Ga Gallium salts (^{68}Ga), and ^{18}F Fluorine (^{18}F), which have been applied to labeling leukocytes and their cellular products, in addition to labeling therapeutic molecules such as antibiotics, monoclonal antibodies, and experimental therapeutics by use of chelator such as diethylene triamine penta-acetic acid (DPTA), 1,4,7,10-tetraazacyclododecane-1, 4, 7, 10-tetraacetic acid (DOTA), and hexamethylpropyleneamine oxime (HMPAO) [2]. The use of such chelators allows for consideration of multiple isotopes due to their ability to modulate the imaging window by compensating for differences in the half-life and function of the isotope (*i.e.*, gamma emission). A summary of the currently available labeling methods and specific details related to their use can be found in Table 1. Other examples require the accumulation of patient derived leukocytes, labeled with ^{111}In -oxine or ^{99m}Tc -HMPAO and re-injected into the donor patient, for the clinical detection of an underlying infection. The current clinical method utilizing labeled leukocytes is recommended for a range of inflammatory disorders and infections; the differentiation between sites of sterile inflammation and infection relies upon optimizing image acquisition and interpretation at pre-determined time points [3–5]. The reliance upon the specificity of image acquisition and interpretation as opposed to the specificity of the reagent highlights the need for pathogen-specific probes as opposed to infection-associated inflammation.

Table 1. Summary of labeling reagents available for pre-clinical and clinical application.

Labeling Agent	Modality	Half-Life	Pre-Clinical	Clinical (FDA approved)
^{99m}Tc Technetium	SPECT	6 h	✓	✓
^{89}Zr Zirconium	PET	3.3 days	✓	✓
67 or ^{68}Ga Gallium salts	PET, SPECT	3.26 days; 68 min	✓	✓
^{111}In Indium	SPECT	2.8 days	✓	✓
^{64}Cu Copper (II)	PET	12.7 h	✓	✓
^{18}F Fluorine	PET	109.8 min	✓	✓
$^{123,124,125,131}\text{I}$ Iodine	PET, SPECT	13.3 h; 4.18 days; 59.4 days; 8 days	✓	✓
Superparamagnetic iron oxide nanoparticles (SPIO)	MRI	N/A	✓	✓
Cross linked iron oxide nanoparticles (CLIO)	MRI	N/A	✓	✓
Monocrystalline iron oxide nanoparticles (MION)	MRI	N/A	✓	✓
Gadolinium-Chelator (DOTA, DPTA, <i>etc.</i>)	MRI	1.5 h	✓	✓
Colloidal Quantum Dots	Optical	N/A	✓	×

Table 1. Cont.

Labeling Agent	Modality	Half-Life	Pre-Clinical	Clinical (FDA approved)
Near-Infrared Fluorophore (NIRF): Indocyanine green	Optical	150–180 s (blood)	✓	✓
Cyanine5, 5.5,7; AlexaFluor dyes	Optical	N/A	✓	×
Bioluminescence	Optical	N/A	✓	×

2. Separating Inflammation from Infection

Discrimination of generalized inflammation from infection is not easily obtained, primarily due to similarities in immune response generated by tissue damage or chronic insult. As a result, currently employed imaging techniques rely largely on the detection of inflammation associated with infection. However, the potential inaccuracy of this assumption limits the efficacy of this approach and necessitates additional confirmation of the underlying infection by positive blood tests or biopsies and non-specific symptoms of the patients, such as fever and general malaise. It is important to note, however, that the identification of immune cells, their receptors, and products, which exhibit up-regulation or increased specificity in the infectious process may be utilized as molecular targets for the monitoring of inflammation associated with infection. Host responses to infectious stimuli trigger overlapping responses that include an initial release of histamines with concurrent elaboration of inflammatory cytokines, followed by a rapid neutrophil burst response to these triggers, prolonged splenic and tissue release of monocytes to the site of damage, tissue conversion of monocytes to macrophages to aid in engulfment and lysis of the foreign pathogens, and later followed by lymphoid generation of pathogen specific T cells and high affinity B cell antibodies. Therefore, we have outlined here a current summary of methods specifically used to detect these immune cell types and their distinguishing products.

2.1. Indirect Detection of Leukocytes

2.1.1. Integrins and Selectins

Although current clinical standards involve the *ex vivo* labeling of patient derived leukocytes, non-invasive methods have been developed to indirectly detect cells through the up regulation of selectin and integrin leukocyte receptors during inflammatory processes. Vascular cell adhesion molecule-1 (VCAM-1) expression is highly up-regulated on endothelial cells as a response to inflammatory cytokines to promote the adhesion of leukocytes, particularly slowing cells rolling from the vasculature, by binding to very late antigen 4 (VLA-4) and subsequent participation in leukocyte-endothelial signal communication. VLA-4 conjugated to VCAM-1 encapsulated in a cross-linked iron oxide nanoparticles (CLIO) has been shown to detect the VCAM-1 expression associated with atherosclerotic plaques [6,7,8]. A molecule similar to VCAM-1, intercellular adhesion molecule 1 (ICAM-1) is displayed by the activated endothelium, macrophages, and lymphocytes upon exposure to the cytokines Interleukin-1 (IL-1) and tumor necrosis factor- α (TNF- α), and allows for the transmigration of leukocytes through the endothelium. To detect relative ICAM-1 levels by MRI, Wong *et al.* developed a superparamagnetic iron

oxide (SPIO)-based nanomicelle coated with lymphocyte function-associated antigen 1 (LFA-1) that binds specifically to ICAM-1 and Choi *et al.* developed a Gd-DPTA-anti-ICAM-1 antibody [9,10].

P-selectin and E-selectin are integrins that are commonly upregulated as a result of inflammation. Imaging of P-selectin has been achieved by several methods: ^{99m}Tc -labeled, ^{111}In -labeled-, and Cy7-labeled-anti-P-selectin monoclonal antibody; fucoidan, a ligand of P-selectin with an affinity in the nanomolar range, has been labeled with ^{99m}Tc ; FITC labeled monoclonal antibody, anti-human CD62P (P-selectin); the development of versatile ultra-small paramagnetic iron oxide nanoparticles (VUSPIO) consisting of PEG and dextran coated iron oxide nanoparticles conjugated with an anti-human-P-selectin monoclonal antibody for MRI; and microparticles of iron oxide with dual ligands of VCAM-1 and P-selectin, also for MRI [11–15]. ^{111}In -labeled and ^{99m}Tc -labeled monoclonal antibodies of E-selectin allow for detection of E-selectin positive immune cells in the inflammatory microenvironment; a comparison of the two methods in a clinical trial of 10 patients with rheumatoid arthritis demonstrated that ^{111}In -labeled and ^{99m}Tc -labeled anti-E-selectin monoclonal antibody have equivalent efficacy in the detection of active inflammation within joints, but ^{99m}Tc is a more readily available radioisotope with a preferred imaging time of four hours [16–18]. A Gd-DPTA nanoparticle with a Sialyl-Lewis^x motif that binds E-selectin was shown to localize to endothelial activation within the brain [19].

2.1.2. Myeloperoxidase

Reporters directed at products elaborated by these immune cells can also be target to assess inflammation that may exist as a result of underlying infection. A central enzyme in inflammatory immune response, myeloperoxidase (MPO), is produced by myeloid cells and generates reactive species, such as hypochlorous acid and oxygen radicals that damage tissues and pathogens. Several agents have been developed that detect MPO and its byproducts; for example, standard hydrogen peroxidase or hydrogen peroxide sensing reagents can be used *in vivo* for this goal. This is typified by the use of luminol as a chemiluminescent light reporter by two MPO dependent mechanisms: The luminol reacts with a radical oxygen produced by NADPH oxidase and is subsequently oxidized by MPO, or it reacts with the hypochlorous acid produced by the reaction of MPO with hydrogen peroxide; each reaction results in the chemiluminescent molecule 3-aminophthalate [20]. A comparable substrate, pholasin, a glycoprotein that reacts with reactive oxygen species (ROS), may be superior to luminol in its method of action due to its increased sensitivity and accelerated degradation [21]. Utilizing two substrates, (DOTA)-Gd and bis-5-HT-DOTA-Gd, that form radicals and oligomers in the presence of MPO, MPO can be detected by MRI as an increase in the relaxivity of the tissue [22]. Sulfonaphthoaminophenyl fluorescein (SNAPF) is a fluorescein probe that responds to the hypochlorous acid produced when MPO catalyzes the oxidation of hydrogen peroxide in the presence of chloride ions in murine and human tissue [23]. Non-specific fluorescein based probes developed for ROS detection include: a naphthofluorescein-based near-infrared fluorescent probe, Naphtho-Peroxyfluor-1 (NPF1), which indicates hydrogen peroxide levels within macrophages as measured by flow cytometry [24]; 2-[6-(4-hydroxy)phenoxy-3H-xanthen-3-on-9-yl]benzoic acid (HPF) and 2-[6-(4-amino)phenoxy-3H-xanthen-3-on-9-yl]benzoic acid (APF) auto-oxidation resistant probes which produce fluorescein upon reaction with specific ROS, and in combination, can discriminate between highly reactive oxygen species and hypochlorite [25]. 5-(and-6)-chloromethyl-2',7'-dichlorodihydrofluorescein diacetate

(CM-H2DCFDA) is a reduced fluorescein probe that permeates the cell, reacts with intracellular ROS, and is retained within the cell (LifeTechnologies).

Potential clinically applicable ROS sensitive probes include antioxidant nanoparticles that degrade into non-toxic and anti-inflammatory components upon exposure to hydrogen peroxide, and then inhibit the generation of ROS by *in vivo* macrophages [26], and a biocompatible nanoparticle coated with 400 quenched oxazine molecules, which are activated upon interaction with peroxyxynitrite and hypochlorous acid produced by MPO [27]. The advantage of imaging MPO reaction products based on the nanoparticle scaffold is that the nanoprobe has a half-life conducive to *in vivo* imaging. In development of the probe, we tested the ability of the MPO sensor to signal inflammatory response in a myocardial infarction model based on permanent ligation of the descending coronary artery. The MPO sensor was given via tail-vein injection at the height of the myeloid inflammatory response and, as the monocytes and neutrophils were recruited to the damaged myocardial, the probe was oxidized by peroxyxynitrite and hypochlorous acid generated in the cells and released into the environment (*i.e.*, oxazine was liberated from the MPO sensor). Although only tested by flow cytometry using neutrophils isolated from splenocytes, this MPO sensor has the ability to respond to hydrazine-based inhibition and may be of use in the evaluation of the *in vivo* efficacy of MPO-based cleavage and heme liberation caused by various hydrazine analogs [28]. MPO is an excellent inflammatory target but would have no ability to discriminate types of pathogens.

2.2. Detection of Myeloid Cells

2.2.1. Monocytes and Macrophages

The differentiation of monocytes to tissue macrophages occurs in the presence of tissue damage or pathogens. Tissue macrophages phagocytose pathogens and apoptotic cells and generate signaling molecules to recruit additional immune cells [29]. Their phagocytic function enables the absorption of iron oxide nanoparticles (CLIO, SPIO, USPIO) [30] and ¹⁹F-labeled-perfluorotributylamine (PFTA) coated particles for MR imaging [31]; additional labeling methods include ⁸⁹Zr-dextran coated nanoparticles (DNP) [32] and ⁶⁴Cu-DTPA-monocrystalline iron oxide nanoparticles (MION) [33], both of which are visualized by hybrid PET/MRI; Macrophage scavenger receptor (MSR) targeted-Gd containing immunomicelles [34] and Gd containing lipid based nanoparticles targeted for the macrophage scavenger receptor-B (CD36) for MR imaging with enhanced macrophage specificity [30,35]. In a comparison study of sterile inflammation and osteomyelitis, injection of USPIO and subsequent macrophage uptake resulted in USPIO-enhanced macrophage localization in infectious vertebral osteomyelitis as opposed to limited macrophage infiltration in sterile vertebral inflammation [36].

2.2.2. Neutrophils

Neutrophils function as key mediators of inflammation and infection due to their phagocytic function and production of ROS in a process termed respiratory burst. Several of the neutrophil specific agents developed utilize the PET agent ^{99m}Tc: ^{99m}Tc-hydrazinonicotinic acid (HYNIC)-Neutrophil activating peptide-2 (NAP-2) [37]; ^{99m}Tc-IL-8 is a chemotactic cytokine secreted by macrophages which binds with strong affinity to receptors on neutrophils [38]; ^{99m}Tc-antiCD15-IgM monoclonal

antibody (LeuTech) binds specifically to both circulating and sequestered neutrophils [39]; leukotriene B-4 (LTB₄), a potent chemoattractant of neutrophils, targeted by ^{99m}Tc-labeled or ¹⁸F-HYNIC-labeled LTB₄ antagonist [40]. In addition to these ^{99m}Tc-labeled targets, two probes have been developed for the formyl peptide receptor displayed by neutrophils: one contains cyanine7 (Cy7) dye conjugated to the formyl peptide mimetic, termed Cy7-PEG-cFIFIFK for pre-clinical fluorescence imaging [41], as well as a cFLFLFK-PEG-⁶⁴Cu-DOTA for MRI [42]. Neutrophils exhibit increased rates of metabolic activity during active infection, and therefore exhibit a high uptake of ¹⁸F-FDG [43], ⁶⁸Gallium salts [44], and indocyanine green (ICG) [45]. In addition, the previously mentioned applications of MPO may also be applied to neutrophils, as MPO constitutes the majority (5%) of their azurophilic granules.

2.3. Adaptive Immunity

The tracking of adaptive immune cells is not a new idea for imaging infection and inflammatory diseases; such studies include appreciation of *in vivo* dendritic cells [46], T cells [47], and B content [48], with recent advancements in the development of contrast agents for MRI [49].

2.3.1. Dendritic Cells

Dendritic cells are professional antigen presenting cells that are present at the initiation of sites of infection and inflammation and then migrate to the lymph nodes and spleen to stimulate the differentiation of B and T cells. Methods developed for the labeling of dendritic cells include: perfluoropolyether labeled dendritic cells that can be detected of ¹⁹F by MRI [50]; a combination of furoxamide and ¹¹¹In-labeled dendritic cells monitored by a combination of SPECT and MRI [51]; these methods have been developed for the non-invasive, long term monitoring of cellular therapy [52–54].

2.3.2. T Cells

T cells are responsible for pathogen immunity by cytolysis of infected cells (CD8+) and activation of B cell affinity maturation (CD4+). Interleukin-2 (IL-2), produced by T cells, stimulates the proliferation of T cells into CD4+ and CD8+ cells; therefore, the detection of IL-2 receptors denotes a pro-inflammatory environment as is consistent with acute infection and chronic inflammatory diseases. To this end, currently PET and SPECT radiopharmaceuticals have been developed: ^{99m}Tc-labeled IL-2 [55,56], ¹⁸F-labeled-IL-2 [57], ³⁵S-labeled IL-2, and ¹²³ or ¹³¹-In-labeled IL-2 [58,59] to detect human activated T lymphocytes [60]. Two CD8+ T cell specific imaging agents have been developed; they each consist of “mini antibodies,” which are derived from parental antibodies specific to primary CD8+ T cells in the peripheral blood, spleen, and lymph nodes. The engineering of mAbs prevents the depletion of CD8+ T cells *in vivo*; these mAbs are then conjugated to S-2-(4-isothiocyanatobenzyl)-1,4,7-triazacyclononane-1,4,7-triacetic acid for ⁶⁴Cu radiolabeling for immuno-PET imaging [61]. T cells and B cells are difficult to label with iron oxide nanoparticles, therefore manganese chloride, a contrast agent that enhances *T₁* relaxivity, may be utilized instead [62]. However, the internalization of the paramagnetic agent decreases the *T₁* relaxivity, reducing the detection strength by MRI.

2.3.3. B Cells

Primary B cell labeling involves the labeling of their cell specific products, antibodies. Monoclonal antibodies have undergone optimization of the radionuclide, the chelating agent, and the antibody construct due to their dual diagnostic and therapeutic ability [63]. In addition to directly labeling antibodies, antibody pre-targeting has been developed. This method consists of an injection of an unlabeled artificial antibody conjugate which binds to a specific antibody, accumulates in the solid tumor (or other area of interest), and then is subsequently imaged by the addition of a high avidity effector molecule that binds to the antibody-conjugate pair. Although this method is currently optimized for oncologic application, the method has relevance to similar infectious disease processes, such as abscesses or other areas of localized infection [64]. Direct labeling of the B cells has been attempted with SPIO nanoparticles in conjugation with NIRF dyes for monitoring B cell dynamics within the spleen. However, the introduction of SPIO nanoparticles appeared to interfere with B cell function, therefore labeling methods require further optimization [65]. In general, the attempts to label a multiplicity of cell types, including B cells, T cells, and dendritic cells are limited to labeling with pre-clinical probes, such as NIRF, GFP, and quantum dots for detection by intravital microscopy or flow cytometry [48]. These methods, though valuable in pre-clinical experimentation, do not provide a promise of translation to clinical application.

2.4. Small Molecule Imaging

2.4.1. Chemokines

Chemokines are a subset of chemotactic cytokines that are secreted at the site of infection or inflammation for the recruitment of immune cells, and therefore have been explored as imaging targets for detection of cell specific immunity [66]. Notably, monocyte chemoattractant protein-1 (MCP-1) has been labeled with ^{125}In allowing for imaging of inflammatory processes which involve monocytes as the primary mediators of inflammation [67]. Another ^{125}In -labeled chemokine, platelet factor-4 (PF-4) synergizes with the interleukin-8 (IL-8) that binds with strong affinity to neutrophil receptors, therefore allowing the visualization of neutrophils in inflammatory processes [68].

2.4.2. Proteases

Imaging protease activity has key benefits to tracking inflammation and infectious disease. Arguably there are three families of proteases that are most often associated: matrix-metalloproteinase (MMP), cathepsins, and caspases. MMPs are zinc dependent proteases capable of degrading extracellular matrices, activating and inactivating chemokines and cytokines, and cleaving ligands and cell surface receptors during cell proliferation, angiogenesis, apoptosis, and cell migration [69]. Broadly, the MMPs family members are classified as collagenase (MMP-1, -8, -13, and -18), gelatinase (MMP-2 and -9), stromelysin (MMP-3, -10, and -11), and matrilysin (MMP-7 and -26). To detect these various MMP subtypes, various probes have been developed: a highly lipophilic ^{111}In or $^{99\text{m}}\text{Tc}$ -DTPA-Cys-Thr-Thr-His-Trp-Gly-Phe-Thr-leu-Cys-OH (^{111}In or $^{99\text{m}}\text{Tc}$ -DTPA-CTT) used to image and inhibit MMP-2 preferentially [70]; a conjugation of an MMP-2 substrate with a quenched

fluorophore released upon substrate recognition and cleavage [71]; a near infrared polymer-based proteolytic beacon “PB-M7NIR,” consisting of a pegylated dendrimer core covalently coupled to a Cy5.5 labeled MMP-7 specific peptide substrate, which preferentially fluoresces in *in vivo* MMP-7 positive tumors relative to a bilateral control tumor [72]. Bremer *et al.* developed a high-density probe conjugated polymer containing a MMP-2 specific substrate that is quenched prior to MMP-2 mediated protease release [73]; PerkinElmer now provides MMPsense, a probe with a broad range of fluorescent labels (AlexaFluor680, 750, *etc.*) and MMP specificity (MMP-2, 3, 7, 9, 12, and 13). A similar method was employed by the group in the development of the Prosense reporter, a pan-cathepsin probe for the detection of cathepsin B, H, or L: PCG (protected graft co-polymer) is conjugated to Cy5.5, which allows the cathepsin to cleave the poly-L-lysine backbone of PCG, releasing the quenched fluorophores of PCG and Cy5.5 [74]. This identical method has been applied to MMPs, caspase-1, cathepsin D, and urokinase plasminogen activator as well.

2.4.3. Caspases

In addition to their involvement in apoptosis, specific caspases, such as caspase-1, 3, and 8 have been identified as activated or inhibited in bacterial and viral infections [75–77]. Targeted photodynamic therapy induces the apoptosis cascade via caspase-9, caspase-8, and caspase-3, and when combined with a caspase-3 activated fluorescent substrate allows for the monitoring of therapeutics [78–80]. Weissleder *et al.* has developed a biocompatible NIR probe which is (ICE)-specific to cleavage by caspase-1 and whose activity has been demonstrated with whole body NIRF imaging [81]. Each of these proteases is united in a common process, apoptosis, and therefore determining their activity provides additional knowledge about the initiation, progression, or cessation of cell death. The probes specifically developed for the detection of apoptotic cells focus on the abnormal cell morphology characteristic of these cells. For example, ^{99m}Tc-labeled bis(zinc(II)-dipicolylamine) (Zn-DPA), a mimetic of annexin V, and annexin V, labeled with one of a variety of reporters including Cy5.5, Gd-DPTA-quantum dot, ¹⁸F, fluorescein isothiocyanate (FITC), or ^{99m}Tc-HYNIC, specifically bind to the phosphatidyl serine exposed on the surface of an apoptotic cell, allowing for the detection of apoptotic cells with multiple imaging modalities [82–87]. Additionally, ¹³¹Iodine labeled peptides are caspase substrates absorbed by apoptotic cells [88].

3. Imaging of Infectious Species

To increase the ease of pre-clinical experimentation, many species of bacteria have been engineered to express a version of the luciferase enzymatic system for the generation of bioluminescence in pre-clinical studies of gene regulation and antibiotic efficacy [89,90]. Standard protocol for clinical imaging of infection utilizes exogenously radiolabeled patient derived leukocytes, in addition to ^{99m}Tc, ⁶⁷Ga, and ¹⁸F-FDG radiopharmaceuticals for PET imaging due to their absorbance by cells exhibiting high metabolic rates; each method therefore localizes to sites of active bacterial infection with increased extravasation and diapedesis of leukocytes. However, these methods mentioned previously cannot differentiate between infection and inflammation, and therefore cannot separate post-operative inflammation or infection, a critical diagnostic difference for therapeutic efficacy.

3.1. Labeled Antimicrobials for Detection of Infection

Synthetic and Endogenous Antibiotics

Labeled antibiotics present a promising method as they localize specifically to the site of an infection, and depending upon their target, are able to identify specific microorganisms. Fluoroquinolones are a class of antibiotics known to intercalate into the DNA of most bacterial species, and therefore have been labeled with ^{99m}Tc and ^{18}F for pet imaging [91–93]. Infecton[®], a ^{99m}Tc -labeled version of ciprofloxacin, is a clinically approved agent that has been shown to have equivalent or greater efficacy in the detection of musculoskeletal bacterial infections as other clinical agents such as ^{18}F -FDG and radiolabeled leukocytes. However, it must be noted that Infecton[®] was removed from the market due to disagreement about the specificity of diagnosis due to incongruity of differentiation between sterile inflammation and infection at multiple time points [91–100]. A specific diagnostic agent for the detection of gram-positive bacteria utilizes magnetic nanoparticles derivatized with vancomycin to form clio-vanco nanoparticles. This method relies on the avidity of the pathogen binding to 10–100s of these iron oxide core sensors resulting in a T_1 -relaxivity change signaling the presence of gram-positive bacteria. These nanoparticles have been specifically shown to identify the Gram-positive bacterium *Staphylococcus aureus* [101,102]. Naturally occurring antibiotic mechanisms, such as antimicrobial peptides and bacteriophages, have also been exploited for imaging by labeling with ^{99m}Tc : this includes the non-specific antimicrobial peptides lactoferrin, defensins, ubiquicidin, and human neutrophil peptide-1 (an α -defensin) and the M13 bacteriophage, which exhibited specificity for bacterial strains of *Escherichia coli* and *Staphylococcus aureus*, and when administered, reduced levels of live *E. coli* in a mouse thigh infection model [103–109]. The high degree of specificity for an intended target and dual diagnostic and therapeutic ability of the ^{99m}Tc -labeled bacteriophage has encouraged the expansion to investigation other phage types [110]. There is a current controversy about the merits and demerits of radiolabeled synthetic antibiotics and endogenous antimicrobial peptides. Briefly, fluoroquinolone antibiotics currently optimized for imaging exhibit a non-preferred accumulation in sterile inflammatory sites, in addition to the concerns about the increasing rise of antibiotic resistance that may generate a false negative diagnosis; however, this method has exhibited a higher degree of specificity than *ex vivo* radiolabeled leukocytes and does not accumulate in the bone marrow, which are important distinctions in the detection of infections such as osteomyelitis, septic arthritis, and infection of orthopedic prostheses. Endogenous antimicrobial peptides exhibit comparable specificity and accuracy to fluoroquinolone antibiotics in the detection of extracellular bacteria, but exhibit none to minimal accumulation in sites of sterile inflammation; however, the greatest concern lies in the development of resistance and subsequent loss of the innate protective mechanism of antimicrobial peptides [111]. A promising antimicrobial peptide, UBI29-41, is a clinically tested agent derived from ubiquicidin, a defensin isolated from human airway epithelial cells. UBI29-41, labeled with ^{99m}Tc , was rigorously tested in animal models, and when translated into Phase I clinical trials showed overall sensitivity, specificity, and accuracy of 100%, 80%, and 94.4%, respectively, in patients with soft tissue infections and osteomyelitis with an optimum time for imaging being 30 min after intravenous administration of the radiopharmaceutical. It was also determined that the detection of the radiopharmaceutical was

dependent on the number of viable bacteria present, as determined after serial treatment with ciprofloxacin; this can be considered as an advantage in determining the efficacy of antibiotic treatment, but a disadvantage in detecting chronic infections with lower numbers of bacteria that may also be encased within biofilms [111–114]. A study conducted compared the specificity of ^{99m}Tc labeled synthetic antimicrobial peptides (UBI 29–41, 18–35, 31–38 and hLf 1–11), human neutrophil peptides (defensins), and ^{99m}Tc -ciprofloxacin (Infecton) in differentiating sites of sterile inflammation and infection [105]. Infection was initiated by injection of multi-drug resistant Gram-positive bacteria (*S. aureus*), Gram-negative bacteria (*Klebsiella pneumoniae*), or fluconazole resistant fungi (*Candida albicans*), while sterile inflammation was induced by injection of heat killed microorganisms or lipopolysaccharide (LPS). Results of this study indicated that antimicrobial peptides accumulated specifically in sites of infection; this is proposed to be due to the preferential binding of these peptides to live microorganisms, not activated host leukocytes. ^{99m}Tc -ciprofloxacin accumulated in sites of sterile inflammation and infection, therefore the authors concluded that ^{99m}Tc -UBI peptides exhibited preferable discrimination of infection from inflammation. This study reinforces the variable ability of ^{99m}Tc -ciprofloxacin to discriminate sterile inflammation from infection; ^{99m}Tc -ciprofloxacin has demonstrated interactions with mammalian cells, including mammalian DNA, DNA gyrase, topoisomerase II, and human leukocytes and endothelial cells, which contributes to the lack of specificity. In addition, the increasing prevalence of drug resistant microorganisms that either subvert the therapeutic mechanism or efflux the molecule limits the binding of labeled drug molecules [115–121].

3.2. Pathogen Specific Targets

In order to optimize the accuracy of imaging clinical infections, targets should include components unique to the infectious species, preferably with species specificity, or specific to the host immune response to infection. Identifying components of the bacterium include the cell wall, bacterial specific enzymes, and specific host factors acquired for growth.

3.2.1. Cell Wall

The unique composition of the bacterial cell wall allows for the development of probes with high specificity. Wheat germ agglutinin, a lectin, conjugated to colloidal quantum dots allows for specific binding to the N-acetylglucosamine and sialic acid of Gram-positive, not Gram-negative, bacterial cell walls [122,123]. Non-specific probes which label both Gram-positive and Gram-negative cell walls include fluorescently labeled D-isomer amino acids which are incorporated into newly synthesized peptidoglycan of bacterial cell walls [124]; ^{111}In -Zn-DPTA and Cyanine-Zn-DPTA have both been shown to bind to bacterial cell walls, for PET and fluorescence imaging respectively [125–127]. In addition, Perkin Elmer has developed Xenolight Rediject bacterial detection probe, a pre-clinical NIRF probe targeted for anionic phospholipids that binds with higher affinity to Gram-negative cell walls, but binds at a comparable concentration to Gram-positive cell walls. For a species-specific diagnostic, SPIO nanoparticles conjugated to an antibody for the cell wall of *Mycobacterium tuberculosis* detect extra pulmonary *M. tuberculosis* infection [128].

3.2.2. Bacterial Specific Factors

Specific co-factors required for bacterial growth have also been exploited for pre-clinical imaging, including targets such as biotin and iron. ^{111}In -DOTA-biotin and zinc-dipicolylamine analog (Zn-DPA)-biotin, non-covalently linked by streptavidin (SA) to form the complex ^{111}In -DOTA-biotin-SA-Zn-DPA-biotin has been developed for enhanced visualization upon bacterial absorption with SPECT-CT imaging [125]. Iron must be seized from the host environment; therefore quantum dots with human transferrin conjugates are internalized by and, therefore, label the bacterium. However, these quantum dots have been shown to increase the survival of *S. aureus* in iron poor environments, and therefore are not applicable in pre-clinical applications [123]. Bacteria also express a thymidine kinase that differs from human thymidine kinase. The radiolabel, ^{124}I -FIAU, is a substrate for the thymidine kinase of bacteria and therefore can be used as an agent to identify musculoskeletal infections by PET-CT [129]. A *S. aureus* specific probe composed of synthetic oligonucleotides flanked by a fluorophore and quencher molecule, termed the Cy5.5-TT probe, was activated upon interaction with the micrococcal nuclease secreted by *S. aureus* [130]. Labeled iron oxide or gold nanoparticles may be absorbed by the bacterium and therefore imaged with MRI, although it is necessary to note that macrophages phagocytosis these particles as well, decreasing the specificity of the diagnosis [131].

4. Endocarditis: A Model of Difficult Diagnosis

Endocarditis is an infection of the heart valve and early detection typifies the need for advancements to promote early diagnosis and assessment of causative microorganism [132]. Initial damage to the heart valve denudes the protective cardiac endothelium leading to a sterile clot, which consists of platelets, coagulation factors, fibrin and, in some areas, basement collagen and stroma. These initial sites of damage are often referred to as “sterile” vegetations. Concurrently, bacteremia by opportunistic pathogens such as *S. aureus* can lead to the formation of bacterial vegetations that weaken the valve, leading to regurgitation and ultimately, heart failure.

Treatment options for patients diagnosed with endocarditis rely heavy on aggressive antibiotic therapy, often lasting up to 4–6 weeks. Although removal of the infected valve may prove necessary, this surgical intervention is complicated by the aforementioned difficulty of diagnosis. Therefore, more discriminatory imaging methods will greatly improve therapeutic efficacy and reduce patient mortality. Guidelines for diagnosis of endocarditis rely on the modified Duke criteria including (i) a fever; (ii) a new heart murrer; (iii) a positive blood culture for *Staphylococcus aureus*, *Streptococcus* species typical of IE, including viridans streptococci and *Streptococcus bovis*, or other microorganisms from persistently positive blood cultures consistent with IE; and (iv) a positive transthoracic or transesophageal echocardiogram (TEE or TTE, respectively) [133,134]. Often serial TEE and TTE are required to determine if there is growth of the fibrin-bacterial-platelet vegetations. These echo-based methods depend on interpretation by a trained radiologist and do not inform on the causative pathogen [135–137]. Therefore, confirmative PET, SPECT, and MRI agents have been developed to complement this traditional method. Table 2 contains a summary of the clinical probes that have been studied for the detection of endocarditis along with useful parameters for discriminating the merit of these findings.

The clinical PET agent ^{18}F -FDG has been shown to identify cardiac vegetations, particularly in cases of prosthetic valve endocarditis (PVE), though high uptake of ^{18}F -FDG in the physiologically normal myocardium remains a concern [138–141]. MRI provides anatomical and functional imaging that allows for the detection of perivalvular abscesses and differentiation of pseudo-aneurysms from infective endocarditis [142]. The majority of the newly developed techniques utilize the SPECT/CT imaging modality. The clinical agent $^{99\text{m}}\text{Tc}$ has been used as a label for HMPAO-WBC (white blood cells), anti-NCA-95, an anti-granulocyte antibody for immunoscintigraphy, stannous pyrophosphate in combination with cardiac scintigraphy, and Annexin V for detection by scintigraphy of platelet activation in experimental endocarditis; ^{111}In has been utilized as a label for platelets and leukocytes with varying success in sensitivity [143–147]. Pre-clinical probes that could be applied for identification of bacteria within the vegetation of IE include synthetic complexes that target the anionic bacterial cell wall [148,149]. The targeting of fibrin within the vegetation, in either non-infective or infective endocarditis, would aid in the detection of lesions missed during serial echocardiography. To this aim, Gd-DPTA nanoparticles coated with anti-fibrin monoclonal antibody were developed and tested in an *in vivo* canine thrombus model; it has also been shown that fibrin targeted antibodies labeled with either ^{111}In or $^{99\text{m}}\text{Tc}$ detected and inhibited the vegetative growth of *Streptococcus sanguinis*. Monoclonal antibodies for fibrin termed GC4 and T2G1, developed by Rosebrough *et.al*, and D59A, developed by Hui *et.al*, labeled with ^{131}I or ^{111}In have been tested in pre-clinical animal studies; D59A has been clinically evaluated for detection for deep vein thrombosis (DVT) (Table 2). These antibodies have been shown to be specific for venous thrombi, due in part to the lack of cross-reactivity with fibrinogen [150–158]. A clinically approved agent, Thromboview[®], is a $^{99\text{m}}\text{Tc}$ labeled humanized monoclonal antibody for the D dimer of cross-linked fibrin utilized for the detection of DVT and pulmonary emboli [159,160]. Two pre-clinical probes specific to coagulase positive *S. aureus*, a major causal agent of infective endocarditis [161–169], have been developed: an AlexaFluor680-Prothrombin (AF680-ProT) analog for near infrared preclinical imaging and a ^{64}Cu -DPTA-Prothrombin (^{64}Cu -DPTA-ProT) analog for use in the more clinically-relevant PET-CT modality [170]. Prothrombin (ProT) is captured and activated by the *S. aureus* secreted proteins, staphylocoagulase and von Willebrand binding protein [171–173]. Staphylocoagulase is secreted into the circulation and also binds through the C-terminal domain to the fibrin deposited in vegetation, and therefore ProT and its analogs, are incorporated into the vegetation on the heart valve. The AF680-ProT analog can be visualized with FMT/CT, while the ^{64}Cu -DPTA-ProT analog requires PET/CT for visualization. Both probes exhibited no effect on the host-clotting cascade while localizing to *S. aureus* vegetations present on heart valves and allowing the monitoring of antibiotic therapy in a murine model of IE. The visualization of a causative microorganism within the vegetation with modified antibiotics has been accomplished by two specific methods: by conjugating vancomycin, an antibiotic which forms hydrogen bonds with the D-alanine moieties present in the Gram-positive cell wall to a fluorochrome, resulting in a probe termed vanco-CW800 for fluorescence imaging; the generation of ^3H -spiramycin, a macrolide antibiotic that inhibits protein synthesis of the bacterium within the vegetation, providing dual diagnostic and therapeutic effect. In addition, Lee *et.al* have developed a miniaturized diagnostic magnetic resonance (DMR) system, containing magnetic nanoparticles conjugated to Vancomycin (CLIO-Vanco sensors), that is able to detect Gram positive bacteria in a small volume of unprocessed sample (10 μL) [102,174,175]. A recently developed probe for

the detection of Enterococci within IE utilizes ^{64}Cu -DOTA-anti pili monoclonal antibody for detection of Enterococci in a model of rat endocarditis by PET/CT. The probe, termed MAb 69, is specific for EbpC region of pili. Pili are implicated in biofilm formation and initiation of endocarditis; therefore, the addition of MAb 69 significantly attenuates the pathogenicity of the Enterococci, coupled with high-density labeling of Enterococci *in vivo* [176]. Those probes described here that have been developed for clinical imaging modalities (*i.e.*, MRI, SPECT, and PET) achieve the high specificity necessary for proper diagnosis of IE, but currently have not been translated to clinical application.

Table 2. A summary of the clinical radiopharmaceuticals applicable to the imaging of endocarditis.

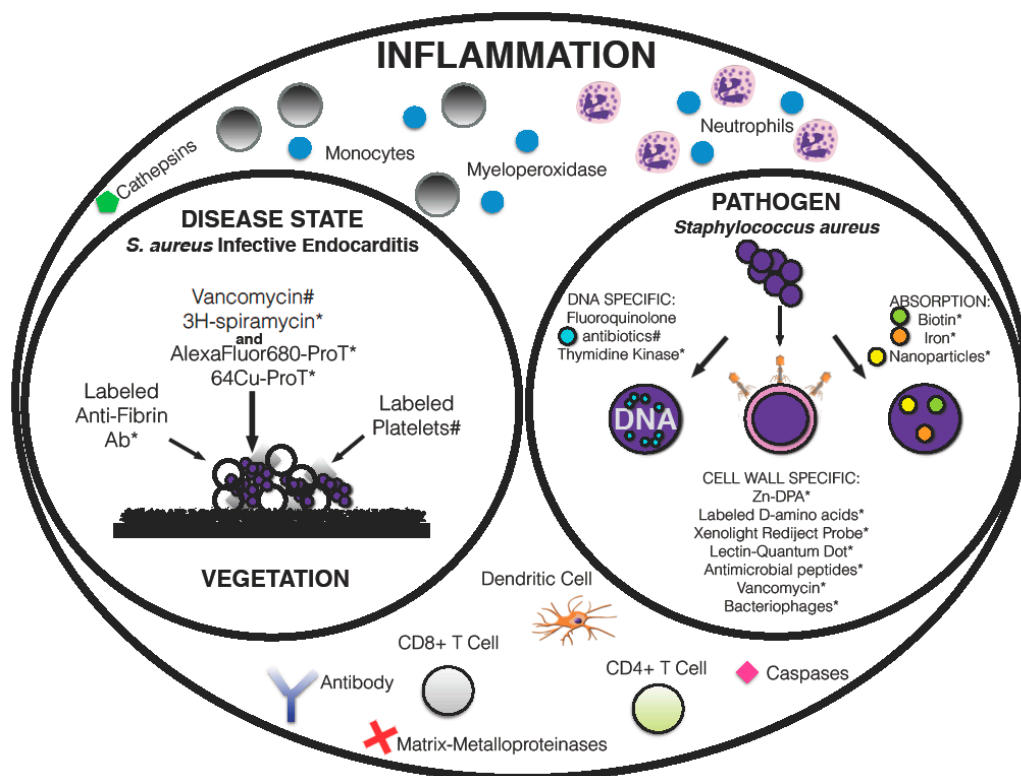
Clinical Tracer	Imaging Modality	Sample Size	Sensitivity	Specificity	Positive and negative predictive values	Evaluated and Recommended for Endocarditis
^{18}F -FDG	PET/CT	72	39%	93%	64% 82%	×
$^{99\text{m}}\text{Tc}$ -HMPAO-WBC	SPECT/CT	51	90%	100%	100% 94%	✓
$^{99\text{m}}\text{Tc}$ -anti-NCA-95	Scintigraphy SPECT	72	79%	82%	×	✓
^{111}In -DTPA-anti-Fibrin mAb	Scintigraphy	86	97%	72%	×	N/A
$^{99\text{m}}\text{Tc}$ -DTPA-anti-Fibrin mAb	Scintigraphy	94	84.2%	97.6%	×	N/A

5. Conclusions

Molecular imaging advancements in technology and targeting have revolutionized pre-clinical discoveries and led to clinical advancements in patient diagnostics. All major disease types have benefited from this revolution or more appropriately evolution of the imaging arts including development of new ways to monitor the pathogenesis of cancer and chronic inflammatory diseases, such as atherosclerosis, diabetes, and autoimmune disorders; application of such advancements to infectious disease would lend an increased specificity to diagnosis that would greatly benefit treatment. Currently, the clinical application of molecular imaging to infection is limited to indirect measurement of enhanced localization and metabolic activity of leukocytes via radiopharmaceuticals for PET or SPECT modalities. The development of diagnostics targeted to the pathogen or disease state would allow the non-invasive identification of the causative microorganism and monitoring of antibiotic therapy for early recognition and eradication of infection. Recently developed diagnostics that satisfy this aim are summarized in Figure 1; $^{99\text{m}}\text{Tc}$ -labeled-Ciprofloxacin (a fluoroquinolone antibiotic) intercalates into bacterial DNA, and as a pathogen targeted detection method demonstrates initial clinical success; however, variability in discrimination between infection and inflammation have initiated its removal from market consideration. The synthetic antimicrobial peptide, UBI 29–41, has demonstrated promising specificity in discriminating infection from inflammation in early clinical trials [104,106–108,112–114]. However, the continued paucity of FDA approved infection specific agents highlights the difficulty of translating pre-clinical to clinical application due to surmounting the barriers of cost, toxicity, and off-target labeling. Therefore, the application of FDA approved materials in a manner specific to the

disease state or pathogen will aid in bypassing the barriers of clinical translation in order to expedite the process of developing infectious disease specific probes. This accelerated method of development is exemplified by the application of USPIO to the diagnosis of vertebral osteomyelitis; it was observed by Bierry *et al.* that two different populations of macrophages infiltrated vertebral osteomyelitis than are found in sterile spinal bone marrow and that injection of USPIO resulted in macrophage uptake and infiltration specific to vertebral osteomyelitis [36]. Targeted methods for specific pathogens would be the most useful for clinical application; however, they are difficult to develop and translate, therefore the novel combination of modalities or probes that are FDA approved may provide a straightforward path for the development of new infectious disease detection agents.

Figure 1. Illustrated within each circle “Inflammation,” “Disease State,” and “Pathogen” are markers that can be utilized as molecular targets in the diagnosis of infection. The identification of general inflammatory markers, depicted in the “Inflammation” circle, indicate the inflammation surrounding an infection, but increased specificity of diagnosis can be gained by focusing on targets associated with a disease state or pathogen. Endocarditis and *Staphylococcus aureus* are depicted here as representative of a disease state and associated pathogen of interest, respectively, with current pre-clinical (*) or clinical (#) applications noted.



Acknowledgments

This work was supported by the National Institutes of Health through grants provided by the National Heart, Lung, and Blood Institute, R00HL094533 (to P.P.) & R01HL114477 (to P.P.), the National Institute of Allergy and Infectious Diseases grant 2R44AI085840-02 (to P.P.).

Author Contributions

H.E wrote the manuscript and created the tables and figures. P.P revised the manuscript as needed and provided suggestions for the formatting and content, as well as final approval of the version to be published.

Conflicts of Interest

The authors declare no conflict of interest.

References

1. Gemmel, F.; Dumarey, N.; Welling, M. Future diagnostic agents. *Semin. Nucl. Med.* **2009**, *39*, 11–26.
2. Goldsmith, S.J.; Vallabhajosula, S. Clinically proven radiopharmaceuticals for infection imaging: Mechanisms and applications. *Semin. Nucl. Med.* **2009**, *39*, 2–10.
3. Palestro, C.J.; Brown, M.L.; Forstrom, L.A.; Greenspan, B.S.; McAfee, J.G.; Royal, H.D.; Schauwecker, D.S.; Seabold, J.E.; Signore, A. *Society of Nuclear Medicine Procedure Guideline for ^{99m}Tc-Exametazime (HMPAO)-Labeled Leukocyte Scintigraphy for Suspected Infection/Inflammation*; The Society of Nuclear Medicine: Reston, VA, USA, 2004.
4. Palestro, C.J.; Brown, M.L.; Forstrom, L.A.; McAfee, J.G.; Royal, H.D.; Schauwecker, D.S.; Seabold, J.E.; Signore, A. *Society of Nuclear Medicine Procedure Guideline for ¹¹¹In-Leukocyte Scintigraphy for Suspected Infection/Inflammation*; The Society of Nuclear Medicine: Reston, VA, USA, 2004.
5. Signore, A. About inflammation and infection. *EJNMMI Res.* **2013**, *3*, 8, doi:10.1186/2191-219X-3-8.
6. Nahrendorf, M.; Jaffer, F.A.; Kelly, K.A.; Sosnovik, D.E.; Aikawa, E.; Libby, P.; Weissleder, R. Noninvasive vascular cell adhesion molecule-1 imaging identifies inflammatory activation of cells in atherosclerosis. *Circulation* **2006**, *114*, 1504–1511.
7. Kelly, K.A.; Nahrendorf, M.; Yu, A.M.; Reynolds, F.; Weissleder, R. *In vivo* phage display selection yields atherosclerotic plaque targeted peptides for imaging. *Mol. Imaging Biol.* **2006**, *8*, 201–207.
8. Kelly, K.A.; Allport, J.R.; Tsourkas, A.; Shinde-Patil, V.R.; Josephson, L.; Weissleder, R. Detection of vascular adhesion molecule-1 expression using a novel multimodal nanoparticle. *Circ. Res.* **2005**, *96*, 327–336.
9. Wong, R.; Chen, X.; Wang, Y.; Hu, X.; Jin, M.M. Visualizing and quantifying acute inflammation using ICAM-1 specific nanoparticles and MRI quantitative susceptibility mapping. *Ann. Biomed. Eng.* **2012**, *40*, 1328–1338.
10. Choi, K.S.; Kim, S.H.; Cai, Q.Y.; Kim, S.Y.; Kim, H.O.; Lee, H.J.; Kim, E.A.; Yoon, S.E.; Yun, K.J.; Yoon, K.H. Inflammation-specific T1 imaging using anti-intercellular adhesion molecule 1 antibody-conjugated gadolinium diethylenetriaminepentaacetic acid. *Mol. Imaging* **2007**, *6*, 75–84.

11. Hariri, G.; Zhang, Y.; Fu, A.; Han, Z.; Brechbiel, M.; Tantawy, M.N.; Peterson, T.E.; Mernaugh, R.; Hallahan, D. Radiation-guided P-selectin antibody targeted to lung cancer. *Ann. Biomed. Eng.* **2008**, *36*, 821–830.
12. Jacobin-Valat, M.J.; Deramchia, K.; Mornet, S.; Hagemeyer, C.E.; Bonetto, S.; Robert, R.; Biran, M.; Massot, P.; Miraux, S.; Sanchez, S.; *et al.* MRI of inducible P-selectin expression in human activated platelets involved in the early stages of atherosclerosis. *NMR Biomed.* **2011**, *24*, 413–424.
13. Ji, S.; Fang, W.; Zhu, M.; Bai, X.; Wang, C.; Ruan, C. Detection of pulmonary embolism with ^{99m}Tc-labeled F(ab)₂ fragment of anti-P-selectin monoclonal antibody in dogs. *Tohoku J. Exp. Med.* **2011**, *223*, 9–15.
14. McAteer, M.A.; Schneider, J.E.; Ali, Z.A.; Warrick, N.; Bursill, C.A.; von zur Muhlen, C.; Greaves, D.R.; Neubauer, S.; Channon, K.M.; Choudhury, R.P. Magnetic resonance imaging of endothelial adhesion molecules in mouse atherosclerosis using dual-targeted microparticles of iron oxide. *Arterioscler. Thrombosis Vasc. Biol.* **2008**, *28*, 77–83.
15. Rouzet, F.; Bachelet-Violette, L.; Alsac, J.M.; Suzuki, M.; Meulemans, A.; Louedec, L.; Petiet, A.; Jandrot-Perrus, M.; Chaubet, F.; Michel, J.B.; *et al.* Radiolabeled fucoidan as a p-selectin targeting agent for *in vivo* imaging of platelet-rich thrombus and endothelial activation. *J. Nucl. Med.* **2011**, *52*, 1433–1440.
16. Jamar, F.; Chapman, P.T.; Harrison, A.A.; Binns, R.M.; Haskard, D.O.; Peters, A.M. Inflammatory arthritis: Imaging of endothelial cell activation with an indium-111-labeled F(ab)₂ fragment of anti-E-selectin monoclonal antibody. *Radiology* **1995**, *194*, 843–850.
17. Jamar, F.; Chapman, P.T.; Manicourt, D.H.; Glass, D.M.; Haskard, D.O.; Peters, A.M. A comparison between ¹¹¹In-anti-E-selectin mAb and ^{99m}Tcm-labelled human non-specific immunoglobulin in radionuclide imaging of rheumatoid arthritis. *Br. J. Radiol.* **1997**, *70*, 473–481.
18. Jamar, F.; Houssiau, F.A.; Devogelaer, J.P.; Chapman, P.T.; Haskard, D.O.; Beaujean, V.; Beckers, C.; Manicourt, D.H.; Peters, A.M. Scintigraphy using a technetium ^{99m}-labelled anti-E-selectin Fab fragment in rheumatoid arthritis. *Rheumatology* **2002**, *41*, 53–61.
19. Sibson, N.R.; Blamire, A.M.; Bernades-Silva, M.; Laurent, S.; Boutry, S.; Muller, R.N.; Styles, P.; Anthony, D.C. MRI detection of early endothelial activation in brain inflammation. *Magn. Reson. Med.* **2004**, *51*, 248–252.
20. Gross, S.; Gammon, S.T.; Moss, B.L.; Rauch, D.; Harding, J.; Heinecke, J.W.; Ratner, L.; Piwnicka-Worms, D. Bioluminescence imaging of myeloperoxidase activity *in vivo*. *Nat. Med.* **2009**, *15*, 455–461.
21. Swindle, E.J.; Hunt, J.A.; Coleman, J.W. A comparison of reactive oxygen species generation by rat peritoneal macrophages and mast cells using the highly sensitive real-time chemiluminescent probe pholasin: Inhibition of antigen-induced mast cell degranulation by macrophage-derived hydrogen peroxide. *J. Immunol.* **2002**, *169*, 5866–5873.
22. Kleijn, A.; Chen, J.W.; Buhrman, J.S.; Wojtkiewicz, G.R.; Iwamoto, Y.; Lamfers, M.L.; Stemmer-Rachamimov, A.O.; Rabkin, S.D.; Weissleder, R.; Martuza, R.L.; *et al.* Distinguishing inflammation from tumor and peritumoral edema by myeloperoxidase magnetic resonance imaging. *Clin. Cancer Res.* **2011**, *17*, 4484–4493.

23. Shepherd, J.; Hilderbrand, S.A.; Waterman, P.; Heinecke, J.W.; Weissleder, R.; Libby, P. A fluorescent probe for the detection of myeloperoxidase activity in atherosclerosis-associated macrophages. *Chem. Biol.* **2007**, *14*, 1221–1231.
24. Albers, A.E.; Dickinson, B.C.; Miller, E.W.; Chang, C.J. A red-emitting naphthofluorescein-based fluorescent probe for selective detection of hydrogen peroxide in living cells. *Bioorg. Med. Chem. Lett.* **2008**, *18*, 5948–5950.
25. Setsukinai, K.; Urano, Y.; Kakinuma, K.; Majima, H.J.; Nagano, T. Development of novel fluorescence probes that can reliably detect reactive oxygen species and distinguish specific species. *J. Biol. Chem.* **2003**, *278*, 3170–3175.
26. Kwon, J.; Kim, J.; Park, S.; Khang, G.; Kang, P.M.; Lee, D. Inflammation-responsive antioxidant nanoparticles based on a polymeric prodrug of vanillin. *Biomacromolecules* **2013**, *14*, 1618–1626.
27. Panizzi, P.; Nahrendorf, M.; Wildgruber, M.; Waterman, P.; Figueiredo, J.L.; Aikawa, E.; McCarthy, J.; Weissleder, R.; Hilderbrand, S.A. Oxazine conjugated nanoparticle detects *in vivo* hypochlorous acid and peroxynitrite generation. *J. Am. Chem. Soc.* **2009**, *131*, 15739–15744.
28. Huang, J.; Smith, F.; Panizzi, P. Ordered cleavage of myeloperoxidase ester bonds releases active site heme leading to inactivation of myeloperoxidase by benzoic acid hydrazide analogs. *Arch. Biochem. Biophys.* **2014**, *548*, 74–85.
29. Murray, P.J.; Wynn, T.A. Protective and pathogenic functions of macrophage subsets. *Nat. Rev. Immunol.* **2011**, *11*, 723–737.
30. Weissleder, R.; Nahrendorf, M.; Pittet, M.J. Imaging macrophages with nanoparticles. *Nat. Mater.* **2014**, *13*, 125–138.
31. Hitchens, T.K.; Ye, Q.; Eytan, D.F.; Janjic, J.M.; Ahrens, E.T.; Ho, C. ¹⁹F MRI detection of acute allograft rejection with *in vivo* perfluorocarbon labeling of immune cells. *Magn. Reson. Med.* **2011**, *65*, 1144–1153.
32. Majmudar, M.D.; Yoo, J.; Keliher, E.J.; Truelove, J.J.; Iwamoto, Y.; Sena, B.; Dutta, P.; Borodovsky, A.; Fitzgerald, K.; di Carli, M.F.; *et al.* Polymeric nanoparticle PET/MR imaging allows macrophage detection in atherosclerotic plaques. *Circ. Res.* **2013**, *112*, 755–761.
33. Nahrendorf, M.; Zhang, H.; Hembrador, S.; Panizzi, P.; Sosnovik, D.E.; Aikawa, E.; Libby, P.; Swirski, F.K.; Weissleder, R. Nanoparticle PET-CT imaging of macrophages in inflammatory atherosclerosis. *Circulation* **2008**, *117*, 379–387.
34. Lipinski, M.J.; Frias, J.C.; Amirbekian, V.; Briley-Saebo, K.C.; Mani, V.; Samber, D.; Abbate, A.; Aguinaldo, J.G.; Massey, D.; Fuster, V.; *et al.* Macrophage-specific lipid-based nanoparticles improve cardiac magnetic resonance detection and characterization of human atherosclerosis. *JACC Cardiovasc. Imaging* **2009**, *2*, 637–647.
35. Amirbekian, V.; Lipinski, M.J.; Briley-Saebo, K.C.; Amirbekian, S.; Aguinaldo, J.G.; Weinreb, D.B.; Vucic, E.; Frias, J.C.; Hyafil, F.; Mani, V.; *et al.* Detecting and assessing macrophages *in vivo* to evaluate atherosclerosis noninvasively using molecular MRI. *Proc. Natl. Acad. Sci. USA* **2007**, *104*, 961–966.
36. Bierry, G.; Jehl, F.; Boehm, N.; Robert, P.; Dietemann, J.L.; Kremer, S. Macrophage imaging by USPIO-enhanced MR for the differentiation of infectious osteomyelitis and aseptic vertebral inflammation. *Eur. Radiol.* **2009**, *19*, 1604–1611.

37. Rennen, H.J.; Frielink, C.; Brandt, E.; Zaat, S.A.; Boerman, O.C.; Oyen, W.J.; Corstens, F.H. Relationship between neutrophil-binding affinity and suitability for infection imaging: Comparison of (99m)Tc-labeled NAP-2 (CXCL-7) and 3 C-terminally truncated isoforms. *J. Nucl. Med.* **2004**, *45*, 1217–1223.
38. Bleeker-Rovers, C.P.; Rennen, H.J.; Boerman, O.C.; Wymenga, A.B.; Visser, E.P.; Bakker, J.H.; van der Meer, J.W.; Corstens, F.H.; Oyen, W.J. 99mTc-labeled interleukin 8 for the scintigraphic detection of infection and inflammation: First clinical evaluation. *J. Nucl. Med.* **2007**, *48*, 337–343.
39. Kipper, S.L.; Rypins, E.B.; Evans, D.G.; Thakur, M.L.; Smith, T.D.; Rhodes, B. Neutrophil-specific 99mTc-labeled anti-CD15 monoclonal antibody imaging for diagnosis of equivocal appendicitis. *J. Nucl. Med.* **2000**, *41*, 449–455.
40. Rennen, H.J.; Laverman, P.; van Eerd, J.E.; Oyen, W.J.; Corstens, F.H.; Boerman, O.C. PET imaging of infection with a HYNIC-conjugated LTB4 antagonist labeled with F-18 via hydrazone formation. *Nucl. Med. Biol.* **2007**, *34*, 691–695.
41. Albertine, K.H.; Gee, M.H. *In vivo* labeling of neutrophils using a fluorescent cell linker. *J. Leukoc. Biol.* **1996**, *59*, 631–638.
42. Locke, L.W.; Chordia, M.D.; Zhang, Y.; Kundu, B.; Kennedy, D.; Landseadel, J.; Xiao, L.; Fairchild, K.D.; Berr, S.S.; Linden, J.; *et al.* A novel neutrophil-specific PET imaging agent: CFLFLFK-PEG-64Cu. *J. Nucl. Med.* **2009**, *50*, 790–797.
43. Sugawara, Y.; Gutowski, T.D.; Fisher, S.J.; Brown, R.S.; Wahl, R.L. Uptake of positron emission tomography tracers in experimental bacterial infections: A comparative biodistribution study of radiolabeled FDG, thymidine, L-methionine, 67Ga-citrate, and 125I-HSA. *Eur. J. Nucl. Med.* **1999**, *26*, 333–341.
44. Tsan, M.F. Mechanism of gallium-67 accumulation in inflammatory lesions. *J. Nucl. Med.* **1985**, *26*, 88–92.
45. Wei, X.; Runnels, J.M.; Lin, C.P. Selective uptake of indocyanine green by reticulocytes in circulation. *Investig. Ophthalmol. Vis. Sci.* **2003**, *44*, 4489–4496.
46. Pham, W.; Xie, J.; Gore, J.C. Tracking the migration of dendritic cells by *in vivo* optical imaging. *Neoplasia* **2007**, *9*, 1130–1137.
47. Fan, Z.; Spencer, J.A.; Lu, Y.; Pitsillides, C.M.; Singh, G.; Kim, P.; Yun, S.H.; Toxavidis, V.; Strom, T.B.; Lin, C.P.; *et al.* *In vivo* tracking of ‘color-coded’ effector, natural and induced regulatory T cells in the allograft response. *Nat. Med.* **2010**, *16*, 718–722.
48. Progatcky, F.; Dallman, M.J.; Lo Celso, C. From seeing to believing: Labelling strategies for *in vivo* cell-tracking experiments. *Interface Focus* **2013**, *3*, 20130001, doi:10.1098/rsfs.2013.0001.
49. Ahrens, E.T.; Bulte, J.W. Tracking immune cells *in vivo* using magnetic resonance imaging. *Nat. Rev. Immunol.* **2013**, *13*, 755–763.
50. Srinivas, M.; Turner, M.S.; Janjic, J.M.; Morel, P.A.; Laidlaw, D.H.; Ahrens, E.T. *In vivo* cytometry of antigen-specific t cells using 19F MRI. *Magn. Reson. Med.* **2009**, *62*, 747–753.
51. de Vries, I.J.; Lesterhuis, W.J.; Barentsz, J.O.; Verdijk, P.; van Krieken, J.H.; Boerman, O.C.; Oyen, W.J.; Bonenkamp, J.J.; Boezeman, J.B.; Adema, G.J.; *et al.* Magnetic resonance tracking of dendritic cells in melanoma patients for monitoring of cellular therapy. *Nat. Biotechnol.* **2005**, *23*, 1407–1413.

52. Arbab, A.S.; Frank, J.A. Cellular MRI and its role in stem cell therapy. *Regen. Med.* **2008**, *3*, 199–215.
53. Klionsky, D.J.; Abeliovich, H.; Agostinis, P.; Agrawal, D.K.; Aliev, G.; Askew, D.S.; Baba, M.; Baehrecke, E.H.; Bahr, B.A.; Ballabio, A.; *et al.* Guidelines for the use and interpretation of assays for monitoring autophagy in higher eukaryotes. *Autophagy* **2008**, *4*, 151–175.
54. Liu, W.; Frank, J.A. Detection and quantification of magnetically labeled cells by cellular MRI. *Eur. J. Radiol.* **2009**, *70*, 258–264.
55. Annovazzi, A.; Biancone, L.; Caviglia, R.; Chianelli, M.; Capriotti, G.; Mather, S.J.; Caprilli, R.; Pallone, F.; Scopinaro, F.; Signore, A. 99mTc-interleukin-2 and (99m)Tc-HMPAO granulocyte scintigraphy in patients with inactive Crohn's disease. *Eur. J. Nucl. Med. Mol. Imaging* **2003**, *30*, 374–382.
56. Annovazzi, A.; Bonanno, E.; Arca, M.; D'Alessandria, C.; Marcocchia, A.; Spagnoli, L.G.; Violi, F.; Scopinaro, F.; de Toma, G.; Signore, A. 99mTc-interleukin-2 scintigraphy for the *in vivo* imaging of vulnerable atherosclerotic plaques. *Eur. J. Nucl. Med. Mol. Imaging* **2006**, *33*, 117–126.
57. Di Galleonardo, V.; Signore, A.; Glaudemans, A.W.; Dierckx, R.A.; de Vries, E.F. N-(4-18F-fluorobenzoyl)interleukin-2 for PET of human-activated T lymphocytes. *J. Nucl. Med.* **2012**, *53*, 679–686.
58. Signore, A.; Annovazzi, A.; Barone, R.; Bonanno, E.; D'Alessandria, C.; Chianelli, M.; Mather, S.J.; Bottoni, U.; Panetta, C.; Innocenzi, D.; *et al.* 99mTc-interleukin-2 scintigraphy as a potential tool for evaluating tumor-infiltrating lymphocytes in melanoma lesions: A validation study. *J. Nucl. Med.* **2004**, *45*, 1647–1652.
59. Signore, A.; Chianelli, M.; Annovazzi, A.; Bonanno, E.; Spagnoli, L.G.; Pozzilli, P.; Pallone, F.; Biancone, L. 123I-interleukin-2 scintigraphy for *in vivo* assessment of intestinal mononuclear cell infiltration in Crohn's disease. *J. Nucl. Med.* **2000**, *41*, 242–249.
60. Signore, A.; Procaccini, E.; Annovazzi, A.; Chianelli, M.; van der Laken, C.; Mire-Sluis, A. The developing role of cytokines for imaging inflammation and infection. *Cytokine* **2000**, *12*, 1445–1454.
61. Tavaré, R.; McCracken, M.N.; Zettlitz, K.A.; Knowles, S.M.; Salazar, F.B.; Olafsen, T.; Witte, O.N.; Wu, A.M. Engineered antibody fragments for immuno-PET imaging of endogenous CD8+ T cells *in vivo*. *Proc. Natl. Acad. Sci. USA* **2014**, *111*, 1108–1113.
62. Aoki, I.; Takahashi, Y.; Chuang, K.H.; Silva, A.C.; Igarashi, T.; Tanaka, C.; Childs, R.W.; Koretsky, A.P. Cell labeling for magnetic resonance imaging with the T1 agent manganese chloride. *NMR Biomed.* **2006**, *19*, 50–59.
63. Weissleder, R.; Gambhir, S.S. *Molecular Imaging: Principles and Practice*; People's Medical Publishing House-USA: Shelton, CT, USA, 2010; p. 1326.
64. Goldenberg, D.M.; Chatal, J.F.; Barbet, J.; Boerman, O.; Sharkey, R.M. Cancer imaging and therapy with bispecific antibody pretargeting. *Update Cancer Ther.* **2007**, *2*, 19–31.
65. Thorek, D.L.; Tsao, P.Y.; Arora, V.; Zhou, L.; Eisenberg, R.A.; Tsourkas, A. *In vivo*, multimodal imaging of B cell distribution and response to antibody immunotherapy in mice. *PLoS One* **2010**, *5*, e10655.

66. Van Eerd, J.E.; Boerman, O.C.; Corstens, F.H.; Oyen, W.J. Radiolabeled chemotactic cytokines: New agents for scintigraphic imaging of infection and inflammation. *Q. J. Nucl. Med.* **2003**, *47*, 246–255.
67. Ohtsuki, K.; Hayase, M.; Akashi, K.; Kopiwoda, S.; Strauss, H.W. Detection of monocyte chemoattractant protein-1 receptor expression in experimental atherosclerotic lesions: An autoradiographic study. *Circulation* **2001**, *104*, 203–208.
68. Rucinski, B.; Knight, L.C.; Niewiarowski, S. Clearance of human platelet factor 4 by liver and kidney: Its alteration by heparin. *Am. J. Physiol.* **1986**, *251*, H800–H807.
69. Page-McCaw, A.; Ewald, A.J.; Werb, Z. Matrix metalloproteinases and the regulation of tissue remodelling. *Nat. Rev. Mol. Cell Biol.* **2007**, *8*, 221–233.
70. Hanaoka, H.; Mukai, T.; Habashita, S.; Asano, D.; Ogawa, K.; Kuroda, Y.; Akizawa, H.; Iida, Y.; Endo, K.; Saga, T.; *et al.* Chemical design of a radiolabeled gelatinase inhibitor peptide for the imaging of gelatinase activity in tumors. *Nucl. Med. Biol.* **2007**, *34*, 503–510.
71. Bremer, C.; Bredow, S.; Mahmood, U.; Weissleder, R.; Tung, C.H. Optical imaging of matrix metalloproteinase-2 activity in tumors: Feasibility study in a mouse model. *Radiology* **2001**, *221*, 523–529.
72. Scherer, R.L.; VanSaun, M.N.; McIntyre, J.O.; Matrisian, L.M. Optical imaging of matrix metalloproteinase-7 activity *in vivo* using a proteolytic nanobeacon. *Mol. Imaging* **2008**, *7*, 118–131.
73. Bremer, C.; Tung, C.H.; Weissleder, R. *In vivo* molecular target assessment of matrix metalloproteinase inhibition. *Nat. Med.* **2001**, *7*, 743–748.
74. Tung, C.H.; Mahmood, U.; Bredow, S.; Weissleder, R. *In vivo* imaging of proteolytic enzyme activity using a novel molecular reporter. *Cancer Res.* **2000**, *60*, 4953–4958.
75. Puri, A.W.; Broz, P.; Shen, A.; Monack, D.M.; Bogoyo, M. Caspase-1 activity is required to bypass macrophage apoptosis upon *Salmonella* infection. *Nat. Chem. Biol.* **2012**, *8*, 745–747.
76. Mocarski, E.S.; Upton, J.W.; Kaiser, W.J. Viral infection and the evolution of caspase 8-regulated apoptotic and necrotic death pathways. *Nat. Rev. Immunol.* **2012**, *12*, 79–88.
77. Man, S.M.; Tourlomousis, P.; Hopkins, L.; Monie, T.P.; Fitzgerald, K.A.; Bryant, C.E. *Salmonella* infection induces recruitment of Caspase-8 to the inflammasome to modulate IL-1beta production. *J. Immunol.* **2013**, *191*, 5239–5246.
78. Chen, Y.; Zheng, W.; Li, Y.; Zhong, J.; Ji, J.; Shen, P. Apoptosis induced by methylene-blue-mediated photodynamic therapy in melanomas and the involvement of mitochondrial dysfunction revealed by proteomics. *Cancer Sci.* **2008**, *99*, 2019–2027.
79. Liu, T.; Wu, L.Y.; Choi, J.K.; Berkman, C.E. Targeted photodynamic therapy for prostate cancer: Inducing apoptosis via activation of the caspase-8/-3 cascade pathway. *Int. J. Oncol.* **2010**, *36*, 777–784.
80. Stefflova, K.; Chen, J.; Marotta, D.; Li, H.; Zheng, G. Photodynamic therapy agent with a built-in apoptosis sensor for evaluating its own therapeutic outcome *in situ*. *J. Med. Chem.* **2006**, *49*, 3850–3856.
81. Messerli, S.M.; Prabhakar, S.; Tang, Y.; Shah, K.; Cortes, M.L.; Murthy, V.; Weissleder, R.; Breakefield, X.O.; Tung, C.H. A novel method for imaging apoptosis using a caspase-1 near-infrared fluorescent probe. *Neoplasia* **2004**, *6*, 95–105.

82. Wyffels, L.; Gray, B.D.; Barber, C.; Moore, S.K.; Woolfenden, J.M.; Pak, K.Y.; Liu, Z. Synthesis and preliminary evaluation of radiolabeled bis(zinc(II)-dipicolylamine) coordination complexes as cell death imaging agents. *Bioorg. Med. Chem.* **2011**, *19*, 3425–3433.
83. Engeland, M.; van den Eijnde, S.M.; Aken, T.; Vermeij-Keers, C.; Ramaekers, F.C.; Schutte, B.; Reutelingsperger, C.P. Detection of apoptosis in ovarian cells *in vitro* and *in vivo* using the annexin V-affinity assay. *Methods Mol. Med.* **2001**, *39*, 669–677.
84. Ntziachristos, V.; Schellenberger, E.A.; Ripoll, J.; Yessayan, D.; Graves, E.; Bogdanov, A., Jr.; Josephson, L.; Weissleder, R. Visualization of antitumor treatment by means of fluorescence molecular tomography with an annexin V-Cy5.5 conjugate. *Proc. Natl. Acad. Sci. USA* **2004**, *101*, 12294–12299.
85. Leung, K. Annexin A5-quantum dot-DTPA-gadolinium. In *Molecular Imaging and Contrast Agent Database (MICAD)*; National Center for Biotechnology Information (US): Bethesda, MD, USA, 2004.
86. D'Arceuil, H.; Rhine, W.; de Crespigny, A.; Yenari, M.; Tait, J.F.; Strauss, W.H.; Engelhorn, T.; Kastrup, A.; Moseley, M.; Blankenberg, F.G. ^{99m}Tc annexin V imaging of neonatal hypoxic brain injury. *Stroke* **2000**, *31*, 2692–2700.
87. Murakami, Y.; Takamatsu, H.; Taki, J.; Tatsumi, M.; Noda, A.; Ichise, R.; Tait, J.F.; Nishimura, S. ¹⁸F-labelled annexin V: A PET tracer for apoptosis imaging. *Eur. J. Nucl. Med. Mol. Imaging* **2004**, *31*, 469–474.
88. Bauer, C.; Bauder-Wuest, U.; Mier, W.; Haberkorn, U.; Eisenhut, M. ¹³¹I-labeled peptides as caspase substrates for apoptosis imaging. *J. Nucl. Med.* **2005**, *46*, 1066–1074.
89. Gahan, C.G. The bacterial lux reporter system: Applications in bacterial localisation studies. *Curr. Gene Ther.* **2012**, *12*, 12–19.
90. Hutchens, M.; Luker, G.D. Applications of bioluminescence imaging to the study of infectious diseases. *Cell. Microbiol.* **2007**, *9*, 2315–2322.
91. Sarda, L.; Saleh-Mghir, A.; Peker, C.; Meulemans, A.; Cremieux, A.C.; Le Guludec, D. Evaluation of (^{99m}Tc)-ciprofloxacin scintigraphy in a rabbit model of *Staphylococcus aureus* prosthetic joint infection. *J. Nucl. Med.* **2002**, *43*, 239–245.
92. Siaens, R.H.; Rennen, H.J.; Boerman, O.C.; Dierckx, R.; Slegers, G. Synthesis and comparison of ^{99m}Tc-enrofloxacin and ^{99m}Tc-ciprofloxacin. *J. Nucl. Med.* **2004**, *45*, 2088–2094.
93. Nayak, D.K.; Baishya, R.; Halder, K.K.; Sen, T.; Sarkar, B.R.; Ganguly, S.; Das, M.K.; Debnath, M.C. Evaluation of (^{99m}Tc(i)-tricarbonyl complexes of fluoroquinolones for targeting bacterial infection. *Metallomics* **2012**, *4*, 1197–1208.
94. Britton, K.E.; Vinjamuri, S.; Hall, A.V.; Solanki, K.; Siraj, Q.H.; Bomanji, J.; Das, S. Clinical evaluation of technetium-^{99m} infecton for the localisation of bacterial infection. *Eur. J. Nucl. Med.* **1997**, *24*, 553–556.
95. Britton, K.E.; Wareham, D.W.; Das, S.S.; Solanki, K.K.; Amaral, H.; Bhatnagar, A.; Katamihardja, A.H.; Malamitsi, J.; Moustafa, H.M.; Soroa, V.E.; *et al.* Imaging bacterial infection with (^{99m}Tc)-ciprofloxacin (Infecton). *J. Clin. Pathol.* **2002**, *55*, 817–823.
96. Hall, A.V.; Solanki, K.K.; Vinjamuri, S.; Britton, K.E.; Das, S.S. Evaluation of the efficacy of ^{99m}Tc-Infecton, a novel agent for detecting sites of infection. *J. Clin. Pathol.* **1998**, *51*, 215–219.

97. Larikka, M.J.; Ahonen, A.K.; Niemela, O.; Puronto, O.; Junila, J.A.; Hamalainen, M.M.; Britton, K.; Syrjala, H.P. ^{99m}Tc-ciprofloxacin (Infecton) imaging in the diagnosis of knee prosthesis infections. *Nucl. Med. Commun.* **2002**, *23*, 167–170.
98. Sarda, L.; Cremieux, A.C.; Lebellec, Y.; Meulemans, A.; Lebtahi, R.; Hayem, G.; Genin, R.; Delahaye, N.; Hutten, D.; le Guludec, D. Inability of ^{99m}Tc-ciprofloxacin scintigraphy to discriminate between septic and sterile osteoarticular diseases. *J. Nucl. Med.* **2003**, *44*, 920–926.
99. Sonmezoglu, K.; Sonmezoglu, M.; Halac, M.; Akgun, I.; Turkmen, C.; Onsel, C.; Kanmaz, B.; Solanki, K.; Britton, K.E.; Uslu, I. Usefulness of ^{99m}Tc-ciprofloxacin (infecton) scan in diagnosis of chronic orthopedic infections: Comparative study with ^{99m}Tc-HMPAO leukocyte scintigraphy. *J. Nucl. Med.* **2001**, *42*, 567–574.
100. Vinjamuri, S.; Hall, A.V.; Solanki, K.K.; Bomanji, J.; Siraj, Q.; O’Shaughnessy, E.; Das, S.S.; Britton, K.E. Comparison of ^{99m}Tc infecton imaging with radiolabelled white-cell imaging in the evaluation of bacterial infection. *Lancet* **1996**, *347*, 233–235.
101. Issadore, D.; Min, C.; Liong, M.; Chung, J.; Weissleder, R.; Lee, H. Miniature magnetic resonance system for point-of-care diagnostics. *Lab Chip* **2011**, *11*, 2282–2287.
102. Lee, H.; Sun, E.; Ham, D.; Weissleder, R. Chip-NMR biosensor for detection and molecular analysis of cells. *Nat. Med.* **2008**, *14*, 869–874.
103. Lupetti, A.; Pauwels, E.K.; Nibbering, P.H.; Welling, M.M. ^{99m}Tc-antimicrobial peptides: Promising candidates for infection imaging. *Q. J. Nucl. Med.* **2003**, *47*, 238–245.
104. Nibbering, P.H.; Welling, M.M.; Paulusma-Annema, A.; Brouwer, C.P.; Lupetti, A.; Pauwels, E.K. ^{99m}Tc-Labeled UBI 29–41 peptide for monitoring the efficacy of antibacterial agents in mice infected with *Staphylococcus aureus*. *J. Nucl. Med.* **2004**, *45*, 321–326.
105. Welling, M.M.; Lupetti, A.; Balter, H.S.; Lanzzeri, S.; Souto, B.; Rey, A.M.; Savio, E.O.; Paulusma-Annema, A.; Pauwels, E.K.; Nibbering, P.H. ^{99m}Tc-labeled antimicrobial peptides for detection of bacterial and *Candida albicans* infections. *J. Nucl. Med.* **2001**, *42*, 788–794.
106. Welling, M.M.; Mongera, S.; Lupetti, A.; Balter, H.S.; Bonetto, V.; Mazzi, U.; Pauwels, E.K.; Nibbering, P.H. Radiochemical and biological characteristics of ^{99m}Tc-UBI 29–41 for imaging of bacterial infections. *Nucl. Med. Biol.* **2002**, *29*, 413–422.
107. Saeed, S.; Zafar, J.; Khan, B.; Akhtar, A.; Qurieshi, S.; Fatima, S.; Ahmad, N.; Irfanullah, J. Utility of (9)(9)^mTc-labelled antimicrobial peptide ubiquicidin (29-41) in the diagnosis of diabetic foot infection. *Eur. J. Nucl. Med. Mol. Imaging* **2013**, *40*, 737–743.
108. Vallejo, E.; Martinez, I.; Tejero, A.; Hernandez, S.; Jimenez, L.; Bialostozky, D.; Sanchez, G.; Ilarraz, H.; Ferro-Flores, G. Clinical utility of ^{99m}Tc-labeled ubiquicidin 29-41 antimicrobial peptide for the scintigraphic detection of mediastinitis after cardiac surgery. *Arch. Med. Res.* **2008**, *39*, 768–774.
109. Rusckowski, M.; Gupta, S.; Liu, G.; Dou, S.; Hnatowich, D.J. Investigations of a (99m)^{Tc}-labeled bacteriophage as a potential infection-specific imaging agent. *J. Nucl. Med.* **2004**, *45*, 1201–1208.
110. Rusckowski, M.; Gupta, S.; Liu, G.; Dou, S.; Hnatowich, D.J. Investigation of four (99m)^{Tc}-labeled bacteriophages for infection-specific imaging. *Nucl. Med. Biol.* **2008**, *35*, 433–440.

111. Akhtar, M.S.; Imran, M.B.; Nadeem, M.A.; Shahid, A. Antimicrobial peptides as infection imaging agents: Better than radiolabeled antibiotics. *Int. J. Pept.* **2012**, *2012*, 965238, doi:10.1155/2012/965238.
112. Akhtar, M.S.; Iqbal, J.; Khan, M.A.; Irfanullah, J.; Jehangir, M.; Khan, B.; Ul-Haq, I.; Muhammad, G.; Nadeem, M.A.; Afzal, M.S.; *et al.* ^{99m}Tc-labeled antimicrobial peptide ubiquicidin (29–41) accumulates less in *Escherichia coli* infection than in *Staphylococcus aureus* infection. *J. Nucl. Med.* **2004**, *45*, 849–856.
113. Akhtar, M.S.; Khan, M.E.; Khan, B.; Irfanullah, J.; Afzal, M.S.; Khan, M.A.; Nadeem, M.A.; Jehangir, M.; Imran, M.B. An imaging analysis of (^{99m}Tc)-UBI (29–41) uptake in *S. aureus* infected thighs of rabbits on ciprofloxacin treatment. *Eur. J. Nucl. Med. Mol. Imaging* **2008**, *35*, 1056–1064.
114. Akhtar, M.S.; Qaisar, A.; Irfanullah, J.; Iqbal, J.; Khan, B.; Jehangir, M.; Nadeem, M.A.; Khan, M.A.; Afzal, M.S.; Ul-Haq, I.; *et al.* Antimicrobial peptide ^{99m}Tc-ubiquicidin 29-41 as human infection-imaging agent: Clinical trial. *J. Nucl. Med.* **2005**, *46*, 567–573.
115. Bisognano, C.; Vaudaux, P.; Rohner, P.; Lew, D.P.; Hooper, D.C. Induction of fibronectin-binding proteins and increased adhesion of quinolone-resistant *Staphylococcus aureus* by subinhibitory levels of ciprofloxacin. *Antimicrob. Agents Chemother.* **2000**, *44*, 1428–1437.
116. Bredberg, A.; Brant, M.; Jaszyk, M. Ciprofloxacin-induced inhibition of topoisomerase II in human lymphoblastoid cells. *Antimicrob. Agents Chemother.* **1991**, *35*, 448–450.
117. Bryant, R.E.; Mazza, J.A. Effect of the abscess environment on the antimicrobial activity of ciprofloxacin. *Am. J. Med.* **1989**, *87*, 23S–27S.
118. Giraud, E.; Cloeckart, A.; Kerboeuf, D.; Chaslus-Dancla, E. Evidence for active efflux as the primary mechanism of resistance to ciprofloxacin in *Salmonella enterica* serovar Typhimurium. *Antimicrob. Agents Chemother.* **2000**, *44*, 1223–1228.
119. Kang, S.L.; Rybak, M.J.; McGrath, B.J.; Kaatz, G.W.; Seo, S.M. Pharmacodynamics of levofloxacin, ofloxacin, and ciprofloxacin, alone and in combination with rifampin, against methicillin-susceptible and -resistant *Staphylococcus aureus* in an *in vitro* infection model. *Antimicrob. Agents Chemother.* **1994**, *38*, 2702–2709.
120. Li, D.; Renzoni, A.; Estoppey, T.; Bisognano, C.; Francois, P.; Kelley, W.L.; Lew, D.P.; Schrenzel, J.; Vaudaux, P. Induction of fibronectin adhesins in quinolone-resistant *Staphylococcus aureus* by subinhibitory levels of ciprofloxacin or by sigma B transcription factor activity is mediated by two separate pathways. *Antimicrob. Agents Chemother.* **2005**, *49*, 916–924.
121. Riesbeck, K.; Andersson, J.; Gullberg, M.; Forsgren, A. Fluorinated 4-quinolones induce hyperproduction of interleukin 2. *Proc. Natl. Acad. Sci. USA* **1989**, *86*, 2809–2813.
122. Kloepfer, J.A.; Mielke, R.E.; Nadeau, J.L. Uptake of CdSe and CdSe/ZnS quantum dots into bacteria *via* purine-dependent mechanisms. *Appl. Environ. Microbiol.* **2005**, *71*, 2548–2557.
123. Kloepfer, J.A.; Mielke, R.E.; Wong, M.S.; Neilson, K.H.; Stucky, G.; Nadeau, J.L. Quantum dots as strain- and metabolism-specific microbiological labels. *Appl. Environ. Microbiol.* **2003**, *69*, 4205–4213.
124. Kuru, E.; Hughes, H.V.; Brown, P.J.; Hall, E.; Tekkam, S.; Cava, F.; de Pedro, M.A.; Brun, Y.V.; VanNieuwenhze, M.S. *In Situ* probing of newly synthesized peptidoglycan in live bacteria with fluorescent D-amino acids. *Angew. Chem.* **2012**, *51*, 12519–12523.

125. Liu, X.; Cheng, D.; Gray, B.D.; Wang, Y.; Akalin, A.; Rusckowski, M.; Pak, K.Y.; Hnatowich, D.J. Radiolabeled Zn-DPA as a potential infection imaging agent. *Nucl. Med. Biol.* **2012**, *39*, 709–714.
126. White, A.G.; Fu, N.; Leevy, W.M.; Lee, J.J.; Blasco, M.A.; Smith, B.D. Optical imaging of bacterial infection in living mice using deep-red fluorescent squaraine rotaxane probes. *Bioconjug. Chem.* **2010**, *21*, 1297–1304.
127. White, A.G.; Gray, B.D.; Pak, K.Y.; Smith, B.D. Deep-red fluorescent imaging probe for bacteria. *Bioorg. Med. Chem. Lett.* **2012**, *22*, 2833–2836.
128. Lee, C.N.; Wang, Y.M.; Lai, W.F.; Chen, T.J.; Yu, M.C.; Fang, C.L.; Yu, F.L.; Tsai, Y.H.; Chang, W.H.; Zuo, C.S.; *et al.* Super-paramagnetic iron oxide nanoparticles for use in extrapulmonary tuberculosis diagnosis. *Clin. Microbiol. Infect.* **2012**, *18*, E149–E157.
129. Diaz, L.A., Jr.; Foss, C.A.; Thornton, K.; Nimmagadda, S.; Endres, C.J.; Uzuner, O.; Seyler, T.M.; Ulrich, S.D.; Conway, J.; Bettgowda, C.; *et al.* Imaging of musculoskeletal bacterial infections by [¹²⁴I]FIAU-PET/CT. *PLoS One* **2007**, *2*, e1007.
130. Hernandez, F.J.; Huang, L.; Olson, M.E.; Powers, K.M.; Hernandez, L.I.; Meyerholz, D.K.; Thedens, D.R.; Behlke, M.A.; Horswill, A.R.; McNamara, J.O., II. Noninvasive imaging of *Staphylococcus aureus* infections with a nuclease-activated probe. *Nat. Med.* **2014**, *20*, 301–306.
131. Depke, M.; Surmann, K.; Hildebrandt, P.; Jehmlich, N.; Michalik, S.; Stanca, S.E.; Fritzsche, W.; Volker, U.; Schmidt, F. Labeling of the pathogenic bacterium *Staphylococcus aureus* with gold or ferric oxide-core nanoparticles highlights new capabilities for investigation of host-pathogen interactions. *Cytom. Part A* **2014**, *85*, 140–150.
132. Bayer, A.S.; Bolger, A.F.; Taubert, K.A.; Wilson, W.; Steckelberg, J.; Karchmer, A.W.; Levison, M.; Chambers, H.F.; Dajani, A.S.; Gewitz, M.H.; *et al.* Diagnosis and management of infective endocarditis and its complications. *Circulation* **1998**, *98*, 2936–2948.
133. Baddour, L.M.; Wilson, W.R.; Bayer, A.S.; Fowler, V.G., Jr.; Bolger, A.F.; Levison, M.E.; Ferrieri, P.; Gerber, M.A.; Tani, L.Y.; Gewitz, M.H.; *et al.* Infective endocarditis: Diagnosis, antimicrobial therapy, and management of complications: A statement for healthcare professionals from the Committee on Rheumatic Fever, Endocarditis, and Kawasaki Disease, Council on Cardiovascular Disease in the Young, and the Councils on Clinical Cardiology, Stroke, and Cardiovascular Surgery and Anesthesia, American Heart Association: Endorsed by the Infectious Diseases Society of America. *Circulation* **2005**, *111*, e394–e434.
134. Li, J.S.; Sexton, D.J.; Mick, N.; Nettles, R.; Fowler, V.G., Jr.; Ryan, T.; Bashore, T.; Corey, G.R. Proposed modifications to the Duke criteria for the diagnosis of infective endocarditis. *Clin. Infect. Dis.* **2000**, *30*, 633–638.
135. Cabell, C.H.; Fowler, V.G., Jr. Repeated echocardiography after the diagnosis of endocarditis: Too much of a good thing? *Heart* **2004**, *90*, 975–976.
136. Chu, V.H.; Bayer, A.S. Use of echocardiography in the diagnosis and management of infective endocarditis. *Curr. Infect. Dis. Rep.* **2007**, *9*, 283–290.
137. Shapiro, S.M.; Bayer, A.S. Transesophageal and Doppler echocardiography in the diagnosis and management of infective endocarditis. *Chest* **1991**, *100*, 1125–1130.

138. Kouijzer, I.J.; Vos, F.J.; Janssen, M.J.; van Dijk, A.P.; Oyen, W.J.; Bleeker-Rovers, C.P. The value of 18F-FDG PET/CT in diagnosing infectious endocarditis. *Eur. J. Nucl. Med. Mol. Imaging* **2013**, *40*, 1102–1107.
139. Moghadam-Kia, S.; Nawaz, A.; Millar, B.C.; Moore, J.E.; Wiegers, S.E.; Torigian, D.A.; Basu, S.; Alavi, A. Imaging with (18)F-FDG-PET in infective endocarditis: Promising role in difficult diagnosis and treatment monitoring. *Hell. J. Nucl. Med.* **2009**, *12*, 165–167.
140. Vind, S.H.; Hess, S. Possible role of PET/CT in infective endocarditis. *J. Nucl. Cardiol.* **2010**, *17*, 516–519.
141. Yen, R.F.; Chen, Y.C.; Wu, Y.W.; Pan, M.H.; Chang, S.C. Using 18-fluoro-2-deoxyglucose positron emission tomography in detecting infectious endocarditis/endoarteritis: A preliminary report. *Acad. Radiol.* **2004**, *11*, 316–321.
142. Vilacosta, I.; Gomez, J. Complementary role of MRI in infectious endocarditis. *Echocardiography* **1995**, *12*, 673–676.
143. Riba, A.L.; Downs, J.; Thakur, M.L.; Gottschalk, A.; Andriole, V.T.; Zaret, B.L. Technetium-99m stannous pyrophosphate imaging of experimental infective endocarditis. *Circulation* **1978**, *58*, 111–119.
144. Riba, A.L.; Thakur, M.L.; Gottschalk, A.; Andriole, V.T.; Zaret, B.L. Imaging experimental infective endocarditis with indium-111-labeled blood cellular components. *Circulation* **1979**, *59*, 336–343.
145. Morguet, A.J.; Munz, D.L.; Ivancevic, V.; Werner, G.S.; Sandrock, D.; Bokemeier, M.; Kreuzer, H. Immunoscintigraphy using technetium-99m-labeled anti-NCA-95 antigranulocyte antibodies as an adjunct to echocardiography in subacute infective endocarditis. *J. Am. Coll. Cardiol.* **1994**, *23*, 1171–1178.
146. Erba, P.A.; Conti, U.; Lazzeri, E.; Sollini, M.; Doria, R.; de Tommasi, S.M.; Bandera, F.; Tascini, C.; Menichetti, F.; Dierckx, R.A.; *et al.* Added value of 99mTc-HMPAO-labeled leukocyte SPECT/CT in the characterization and management of patients with infectious endocarditis. *J. Nucl. Med.* **2012**, *53*, 1235–1243.
147. Rouzet, F.; Dominguez Hernandez, M.; Hervatin, F.; Sarda-Mantel, L.; Lefort, A.; Duval, X.; Louedec, L.; Fantin, B.; le Guludec, D.; Michel, J.B. Technetium 99m-labeled annexin V scintigraphy of platelet activation in vegetations of experimental endocarditis. *Circulation* **2008**, *117*, 781–789.
148. Leevy, W.M.; Gammon, S.T.; Jiang, H.; Johnson, J.R.; Maxwell, D.J.; Jackson, E.N.; Marquez, M.; Piwnica-Worms, D.; Smith, B.D. Optical imaging of bacterial infection in living mice using a fluorescent near-infrared molecular probe. *J. Am. Chem. Soc.* **2006**, *128*, 16476–16477.
149. Leevy, W.M.; Gammon, S.T.; Johnson, J.R.; Lampkins, A.J.; Jiang, H.; Marquez, M.; Piwnica-Worms, D.; Suckow, M.A.; Smith, B.D. Noninvasive optical imaging of *Staphylococcus aureus* bacterial infection in living mice using a Bis-dipicolylamine-Zinc(II) affinity group conjugated to a near-infrared fluorophore. *Bioconjug. Chem.* **2008**, *19*, 686–692.
150. Flacke, S.; Fischer, S.; Scott, M.J.; Fuhrhop, R.J.; Allen, J.S.; McLean, M.; Winter, P.; Sicard, G.A.; Gaffney, P.J.; Wickline, S.A.; *et al.* Novel MRI contrast agent for molecular imaging of fibrin: Implications for detecting vulnerable plaques. *Circulation* **2001**, *104*, 1280–1285.

151. Yokota, M.; Basi, D.L.; Herzberg, M.C.; Meyer, M.W. Anti-fibrin antibody binding in valvular vegetations and kidney lesions during experimental endocarditis. *Microbiol. Immunol.* **2001**, *45*, 699–707.
152. Hui, K.Y.; Haber, E.; Matsueda, G.R. Immunodetection of human fibrin using monoclonal antibody-64C5 in an extracorporeal chicken model. *Thromb. Haemost.* **1985**, *54*, 524–527.
153. Hui, K.Y.; Haber, E.; Matsueda, G.R. Monoclonal antibodies of predetermined specificity for fibrin: A rational approach to monoclonal antibody production. *Hybridoma* **1986**, *5*, 215–222.
154. Rosebrough, S.F.; Grossman, Z.D.; McAfee, J.G.; Kudryk, B.J.; Subramanian, G.; Ritter-Hrncirik, C.A.; Witanowski, L.S.; Tillapaugh-Fay, G.; Urrutia, E. Aged venous thrombi: Radioimmunoimaging with fibrin-specific monoclonal antibody. *Radiology* **1987**, *162*, 575–577.
155. Rosebrough, S.F.; Grossman, Z.D.; McAfee, J.G.; Kudryk, B.J.; Subramanian, G.; Ritter-Hrncirik, C.A.; Witanowski, L.S.; Tillapaugh-Fay, G.; Urrutia, E.; Zapf-Longo, C. Thrombus imaging with indium-111 and iodine-131-labeled fibrin-specific monoclonal antibody and its F(ab')₂ and Fab fragments. *J. Nucl. Med.* **1988**, *29*, 1212–1222.
156. Rosebrough, S.F.; McAfee, J.G.; Grossman, Z.D.; Kudryk, B.J.; Ritter-Hrncirik, C.A.; Witanowski, L.S.; Maley, B.L.; Bertrand, E.A.; Gagne, G.M. Thrombus imaging: A comparison of radiolabeled GC4 and T2G1s fibrin-specific monoclonal antibodies. *J. Nucl. Med.* **1990**, *31*, 1048–1054.
157. Rosebrough, S.F.; McAfee, J.G.; Grossman, Z.D.; Schemancik, L.A. Immunoreactivity of 111In and 131I fibrin-specific monoclonal antibody used for thrombus imaging. *J. Immunol. Methods* **1989**, *116*, 123–129.
158. Alavi, A.; Gupta, N.; Palevsky, H.I.; Kelley, M.A.; Jatlow, A.D.; Byar, A.A.; Berger, H.J. Detection of thrombophlebitis with 111In-labeled anti-fibrin antibody: Preliminary results. *Cancer Res.* **1990**, *50*, 958s–961s.
159. Douketis, J.D.; Ginsberg, J.S.; Haley, S.; Julian, J.; Dwyer, M.; Levine, M.; Eisenberg, P.R.; Smart, R.; Tsui, W.; White, R.H.; *et al.* Accuracy and safety of (99m)Tc-labeled anti-D-dimer (DI-80B3) Fab' fragments (ThromboView(R)) in the diagnosis of deep vein thrombosis: A phase II study. *Thromb. Res.* **2012**, *130*, 381–389.
160. Morris, T.A.; Gerometta, M.; Yusen, R.D.; White, R.H.; Douketis, J.D.; Kaatz, S.; Smart, R.C.; Macfarlane, D.; Ginsberg, J.S. Detection of pulmonary emboli with 99mTc-labeled anti-D-dimer (DI-80B3)Fab' fragments (ThromboView). *Am. J. Respir. Crit. Care Med.* **2011**, *184*, 708–714.
161. Federspiel, J.J.; Stearns, S.C.; Peppercorn, A.F.; Chu, V.H.; Fowler, V.G., Jr. Increasing US rates of endocarditis with *Staphylococcus aureus*: 1999–2008. *Arch. Intern. Med.* **2012**, *172*, 363–365.
162. Fortes, C.Q.; Espanha, C.A.; Bustorff, F.P.; Zappa, B.C.; Ferreira, A.L.; Moreira, R.B.; Pereira, N.G.; Fowler, V.G., Jr.; Deshmukh, H. First reported case of infective endocarditis caused by community-acquired methicillin-resistant *Staphylococcus aureus* not associated with healthcare contact in Brazil. *Braz. J. Infect. Dis.* **2008**, *12*, 541–543.
163. Fowler, V.G., Jr.; Miro, J.M.; Hoen, B.; Cabell, C.H.; Abrutyn, E.; Rubinstein, E.; Corey, G.R.; Spelman, D.; Bradley, S.F.; Barsic, B.; *et al.* *Staphylococcus aureus* endocarditis: A consequence of medical progress. *JAMA* **2005**, *293*, 3012–3021.

164. Fowler, V.G., Jr.; Sanders, L.L.; Kong, L.K.; McClelland, R.S.; Gottlieb, G.S.; Li, J.; Ryan, T.; Sexton, D.J.; Roussakis, G.; Harrell, L.J.; *et al.* Infective endocarditis due to *Staphylococcus aureus*: 59 prospectively identified cases with follow-up. *Clin. Infect. Dis.* **1999**, *28*, 106–114.
165. Miro, J.M.; Anguera, I.; Cabell, C.H.; Chen, A.Y.; Stafford, J.A.; Corey, G.R.; Olaison, L.; Eykyn, S.; Hoen, B.; Abrutyn, E.; *et al.* *Staphylococcus aureus* native valve infective endocarditis: Report of 566 episodes from the International Collaboration on Endocarditis Merged Database. *Clin. Infect. Dis.* **2005**, *41*, 507–514.
166. Nienaber, J.J.; Sharma Kuinkel, B.K.; Clarke-Pearson, M.; Lamletthson, S.; Park, L.; Rude, T.H.; Barriere, S.; Woods, C.W.; Chu, V.H.; Marin, M.; *et al.* Methicillin-susceptible *Staphylococcus aureus* endocarditis isolates are associated with clonal complex 30 genotype and a distinct repertoire of enterotoxins and adhesins. *J. Infect. Dis.* **2011**, *204*, 704–713.
167. Petti, C.A.; Fowler, V.G., Jr. *Staphylococcus aureus* bacteremia and endocarditis. *Infect. Dis. Clin. N. Am.* **2002**, *16*, 413–435, x–xi.
168. Rasmussen, R.V.; Host, U.; Arpi, M.; Hassager, C.; Johansen, H.K.; Korup, E.; Schonheyder, H.C.; Berning, J.; Gill, S.; Rosenvinge, F.S.; *et al.* Prevalence of infective endocarditis in patients with *Staphylococcus aureus* bacteraemia: The value of screening with echocardiography. *Eur. J. Echocardiogr.* **2011**, *12*, 414–420.
169. Petti, C.A.; Fowler, V.G., Jr. *Staphylococcus aureus* bacteremia and endocarditis. *Infect. Dis. Clin. N. Am.* **2002**, *16*, 413–435, x–xi.
170. Panizzi, P.; Nahrendorf, M.; Figueiredo, J.L.; Panizzi, J.R.; Marinelli, B.; Iwamoto, Y.; Keliher, E.; Maddur, A.A.; Waterman, P.; Kroh, H.K. *et al.* *In Vitro* detection of *Staphylococcus aureus* endocarditis by targeting pathogen-specific prothrombin activation. *Nat. Med.* **2011**, *17*, 1142–1146.
171. Friedrich, R.; Panizzi, P.; Fuentes-Prior, P.; Richter, K.; Verhamme, I.; Anderson, P.J.; Kawabata, S.; Huber, R.; Bode, W.; Bock, P.E. Staphylocoagulase is a prototype for the mechanism of cofactor-induced zymogen activation. *Nature* **2003**, *425*, 535–539.
172. Kroh, H.K.; Panizzi, P.; Bock, P.E. Von Willebrand factor-binding protein is a hysteretic conformational activator of prothrombin. *Proc. Natl. Acad. Sci. USA* **2009**, *106*, 7786–7791.
173. Panizzi, P.; Friedrich, R.; Fuentes-Prior, P.; Kroh, H.K.; Briggs, J.; Tans, G.; Bode, W.; Bock, P.E. Novel fluorescent prothrombin analogs as probes of staphylocoagulase–prothrombin interactions. *J. Biol. Chem.* **2006**, *281*, 1169–1178.
174. Van Oosten, M.; Schafer, T.; Gazendam, J.A.; Ohlsen, K.; Tsompanidou, E.; de Goffau, M.C.; Harmsen, H.J.; Crane, L.M.; Lim, E.; Francis, K.P.; *et al.* Real-time *in vivo* imaging of invasive- and biomaterial-associated bacterial infections using fluorescently labelled vancomycin. *Nat. Commun.* **2013**, *4*, 2584, doi:10.1038/ncomms3584.
175. Cremieux, A.C.; Vallois, J.M.; Maziere, B.; Ottaviani, M.; Bouvet, A.; Carbon, C.; Pocardalo, J.J. 3H-spiramycin penetration into fibrin vegetations in an experimental model of streptococcal endocarditis. *J. Antimicrob. Chemother.* **1988**, *22* (Suppl. B), 127–133.

176. Pinkston, K.L.; Singh, K.V.; Gao, P.; Wilganowski, N.; Robinson, H.; Ghosh, S.; Azhdarinia, A.; Sevick-Muraca, E.M.; Murray, B.E.; Harvey, B.R. Targeting pili in enterococcal pathogenesis. *Infect. Immun.* **2014**, *82*, 1540–1547.

© 2014 by the authors; licensee MDPI, Basel, Switzerland. This article is an open access article distributed under the terms and conditions of the Creative Commons Attribution license (<http://creativecommons.org/licenses/by/3.0/>).